

Topic	Additional seismogram examples within the distance range 13° - 100°
compiled by	Klaus Klinge, Federal Institute for Geosciences and Natural Resources, Seismological Central Observatory, Gräfenberg (SZGRF), Mozartstrasse 57, 91052 Erlangen, Germany, Fax: +49 9131 8104 099, E-mail: klinge@szgrf.bgr.de
Version	October, 2001

Note: Most of the examples given below show either records of the German Regional Seismic Network (GRSN; aperture about 500 x 800 km) or of the Gräfenberg broadband array (GRF; aperture 45 x 110 km; see Figs. 8.14 and 9.4 in the manual Chapters 8 and 9). The following abbreviations have been used: D – epicentral distance in degree, BAZ – backazimuth in degree, h – focal depth in kilometer. Complementary comments have been added by the Editor.

Example 1: Earthquake in Greece

USGS NEIC-data:1999-09-07 OT 11:56:50 38.13N 23.55E h = 10km mb = 5.8

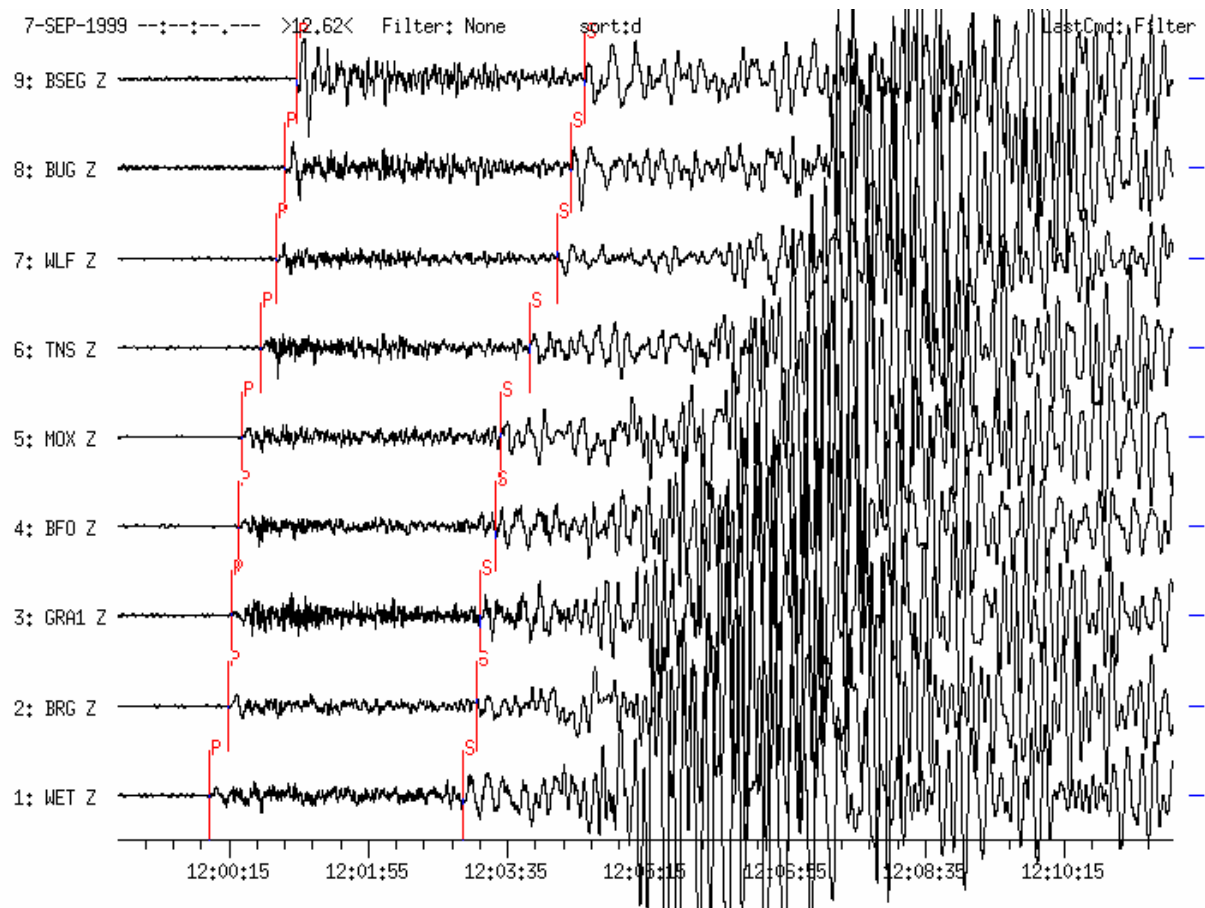


Figure 1a Broadband vertical-component seismograms recorded at 9 GRF/GRSN stations within the distance range $D = 13.4^\circ$ (WET) to 18.2° (BSEG). Traces have been sorted according to increasing distance. A complex P wave is followed by S and surface waves with longer-periods than P. Both body waves are influenced by upper mantle discontinuities. Note the large P-wave amplitude at the most distant station BSEG because amplitudes increase rapidly towards the “20° discontinuity” (see Fig. 3.13 in Chapter 3).

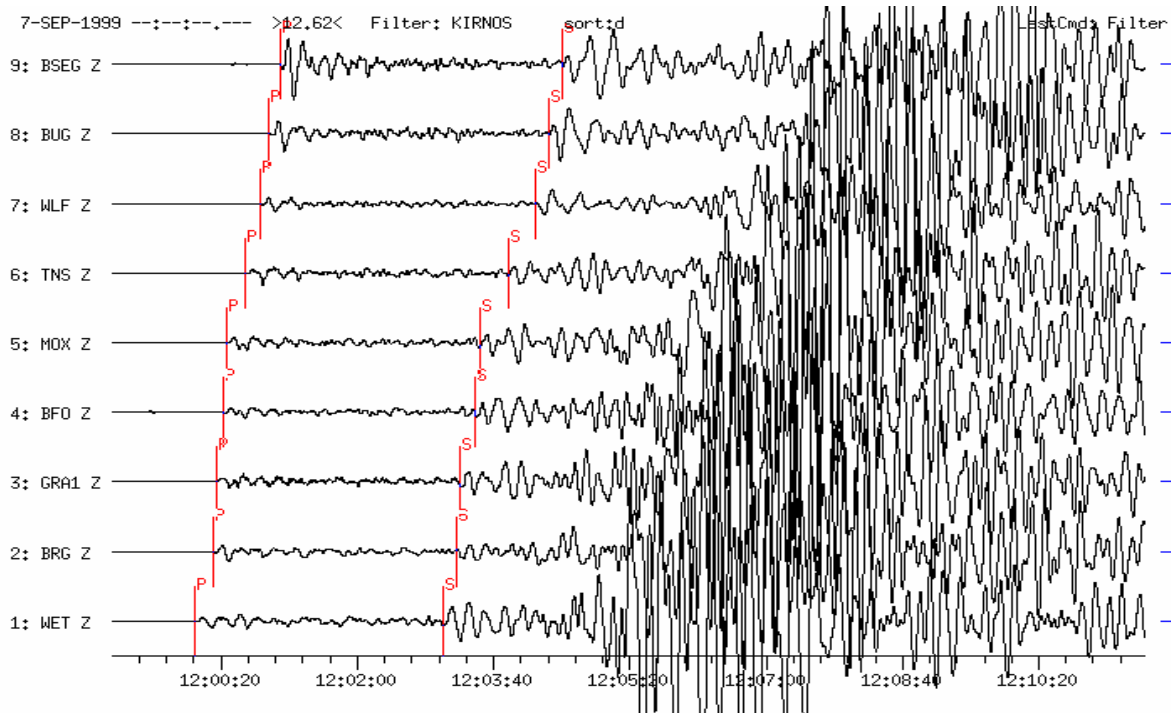


Figure 1b The same record as above, however a displacement proportional KIRNOS-filter was applied. Especially S waves are displayed better by using this filter. The network traces are not coherent.

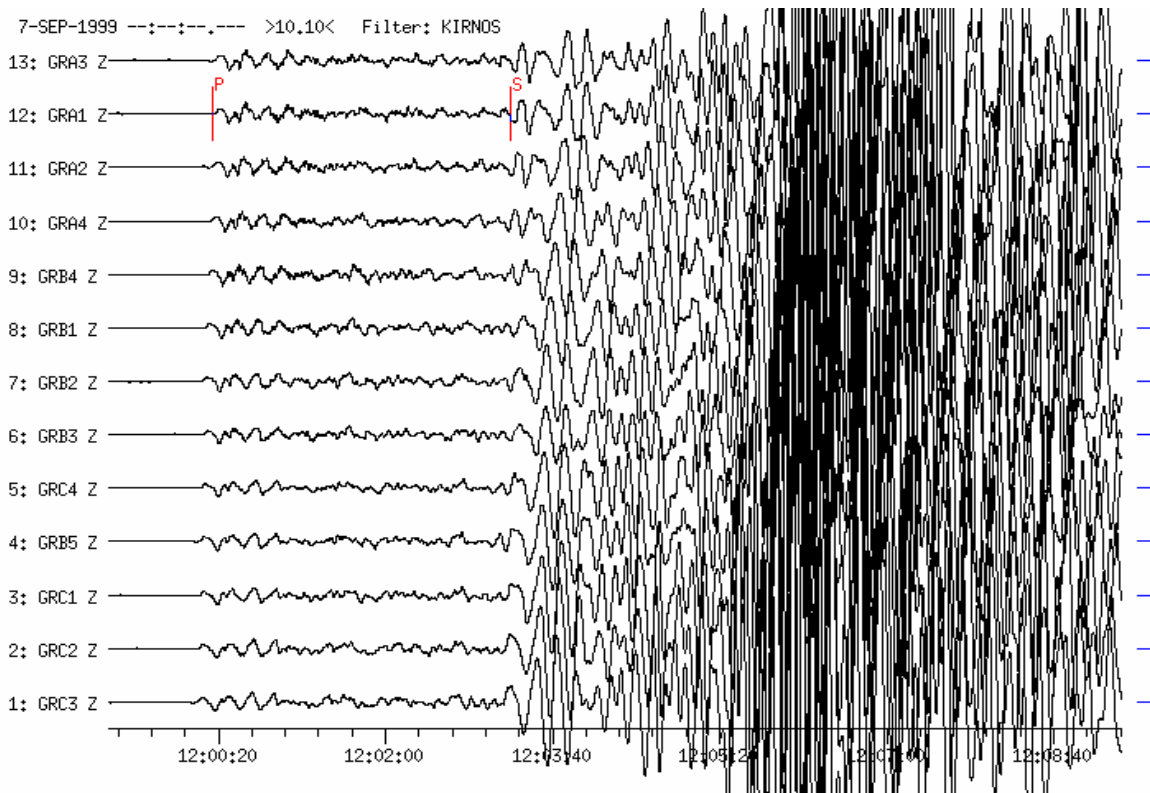


Figure 1c KIRNOS-filtered seismograms of vertical-component records at the GRF-array stations sorted according to increasing epicentral distance ($D = 13.8^\circ$ to GRC3 and 14.6° to GRA3). Note the variability of waveforms within the S-wave group.

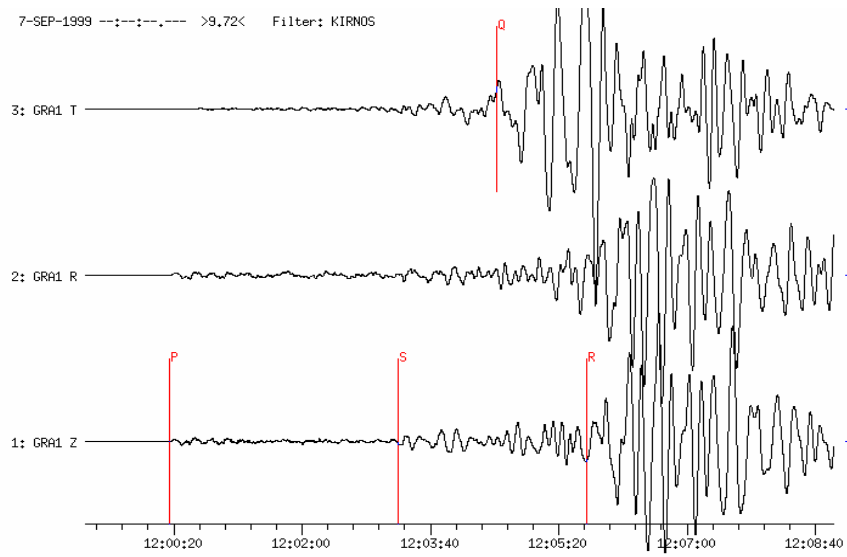


Figure 1d KIRNOS-filtered three-component seismogram from the GRF-array station GRA1 ($D = 14.55^\circ$, $BAZ = 138^\circ$). The horizontal components N and E have been rotated into the radial (R) and transverse (T) direction. The onsets of the body waves P and S and of the long-period surface waves LQ (Q) and LR (R) have been marked.

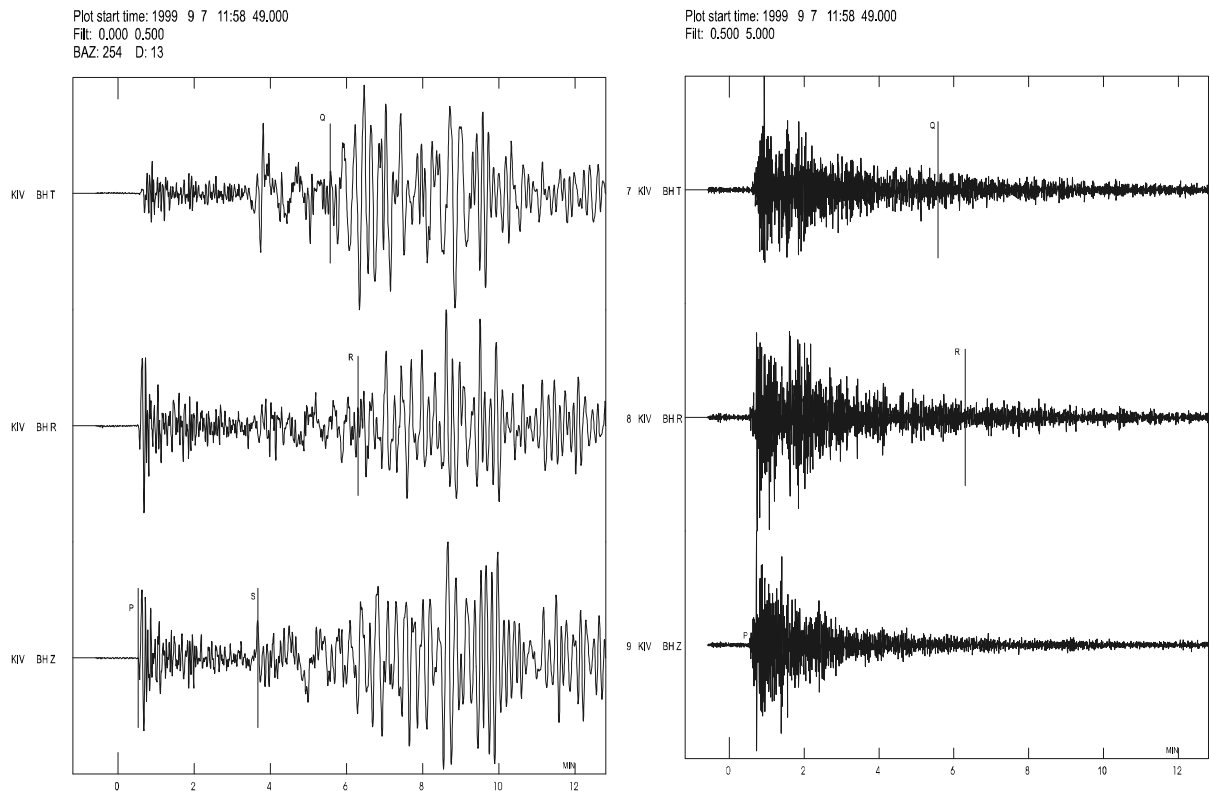
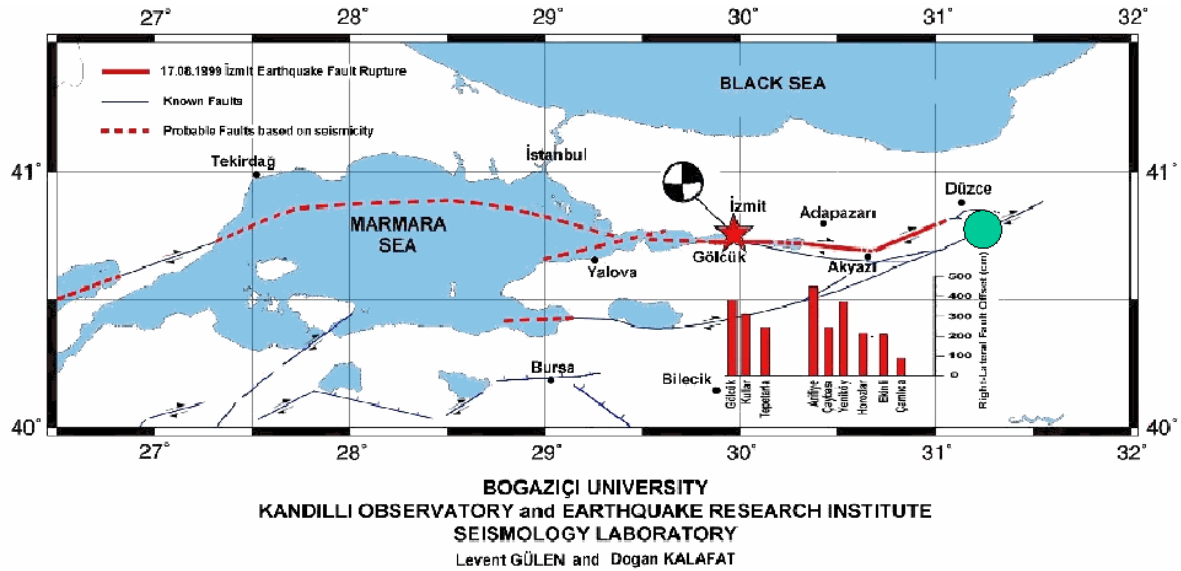


Figure 1e Low-pass (left) and high-frequency band-pass filtered (0.5-5 Hz) seismograms of the same earthquake recorded at station KIV (Kislovodsk; Russia) at the distance $D = 15.2^\circ$. The horizontal components N and E have been rotated into the R and T direction. No long-period waves are visible in the high-frequency record (courtesy of Lars Ottemöller, 2002).

Example 2: Earthquake in NW-TURKEY

USGS NEIC-data:1999-11-12 OT 16:57:20 40.79N 31.11E h = 10km Mw = 7.1
(D = 16.5° to GRF, BAZ = 115°)




 12.11.1999 Mw 7.1 (NEIC)

Figure 2a The Düzce earthquake of November 12, 1999 occurred about 110 km east of the earlier Izmit earthquake of August 17, 1999. The map shows the epicenter regions of both earthquakes together with one moment-tensor solution (for the Izmit event) and the right lateral surface displacement values (in cm) observed after the first shock.

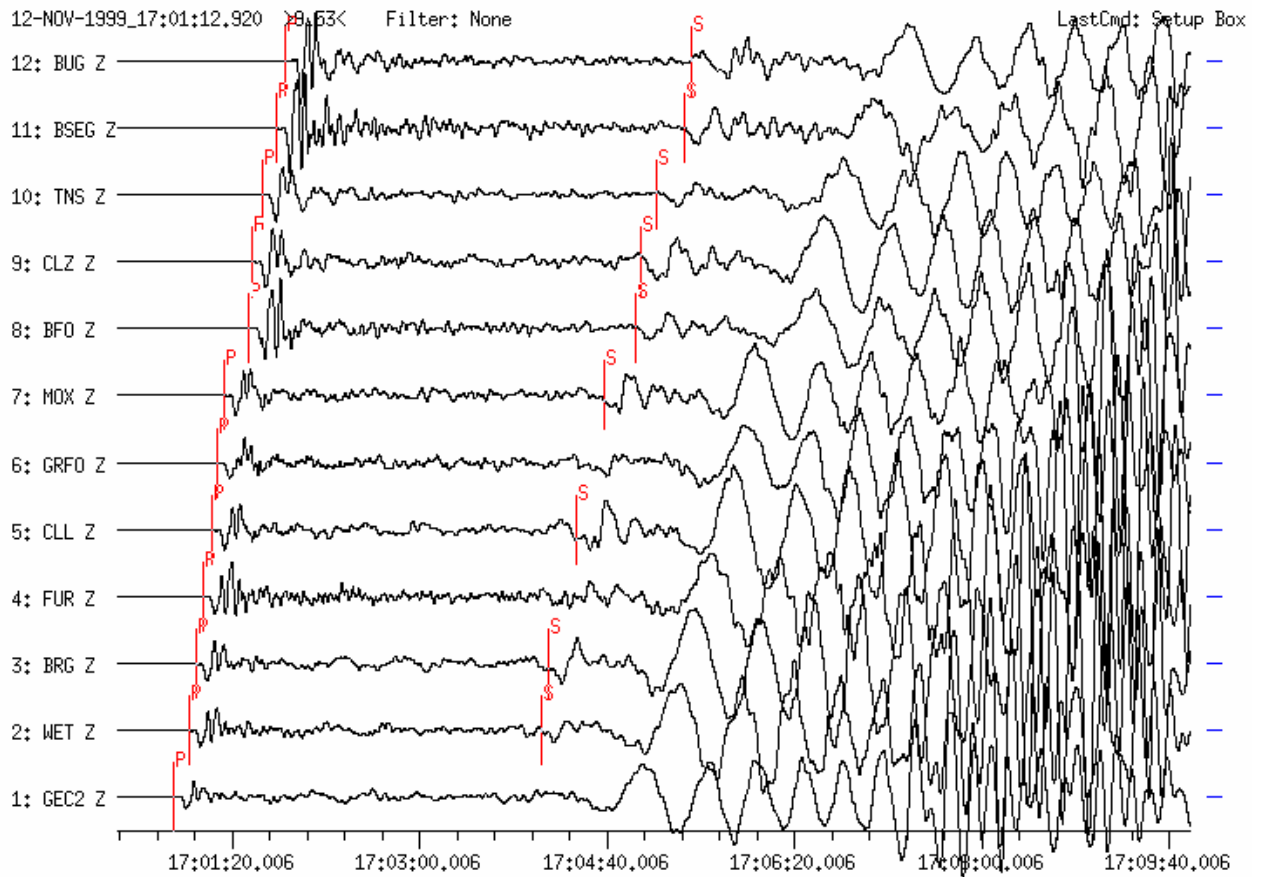


Figure 2b Broadband vertical-component seismograms recorded at 12 GRSN stations. Traces are sorted according to increasing distance ($D = 14.7^\circ$ from GEC2 and 19.6° from BUG). A clear P wave is followed by a relatively weak S and strong dispersed surface waves with much longer-periods than P. The P and S waveforms, influenced by upper mantle discontinuities, show a complicated structure. Note the growing P-wave complexity and amplitudes with increasing distance towards the “20° discontinuity” (see Fig. 2.29 in Chapter 2 and Fig. 3.13 in Chapter 3).

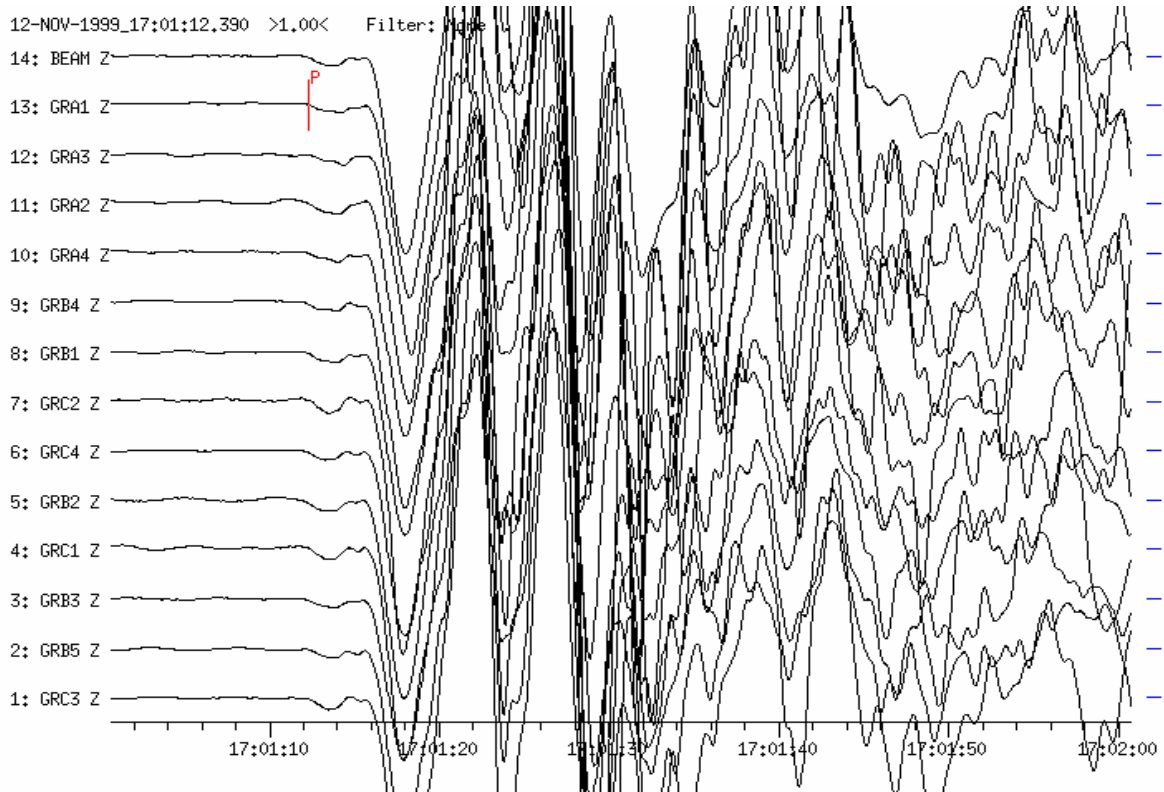


Figure 2c Broadband vertical-component seismogram with P-wave onsets recorded at all GRF-array stations. Traces are sorted according to increasing distance ($D = 12.86^\circ$ from GRC3 and 13.03° from GRA1) and shifted in time according to a reference station (beamforming). All signal onsets are coherent. The weak first arrival of the P-wave onset is marked on the GRF-station GRA1.

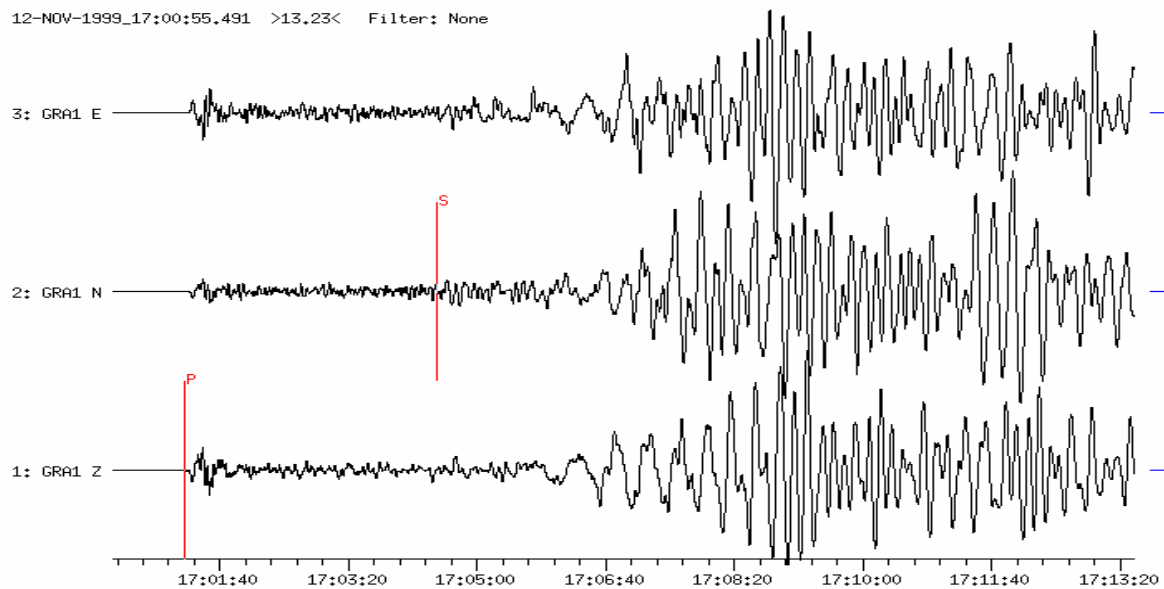


Figure 2d Broadband seismogram with P, weak S and long-period surface waves from station GRA1 (at $D = 13.0^\circ$).

Example 3: Earthquake in Southern TURKEY

USGS QED-data: 1998-06-27 OT 13:55:49 36.95N 35.31E h = 10G Ms = 6.2
(D = 21.6° to GRF)

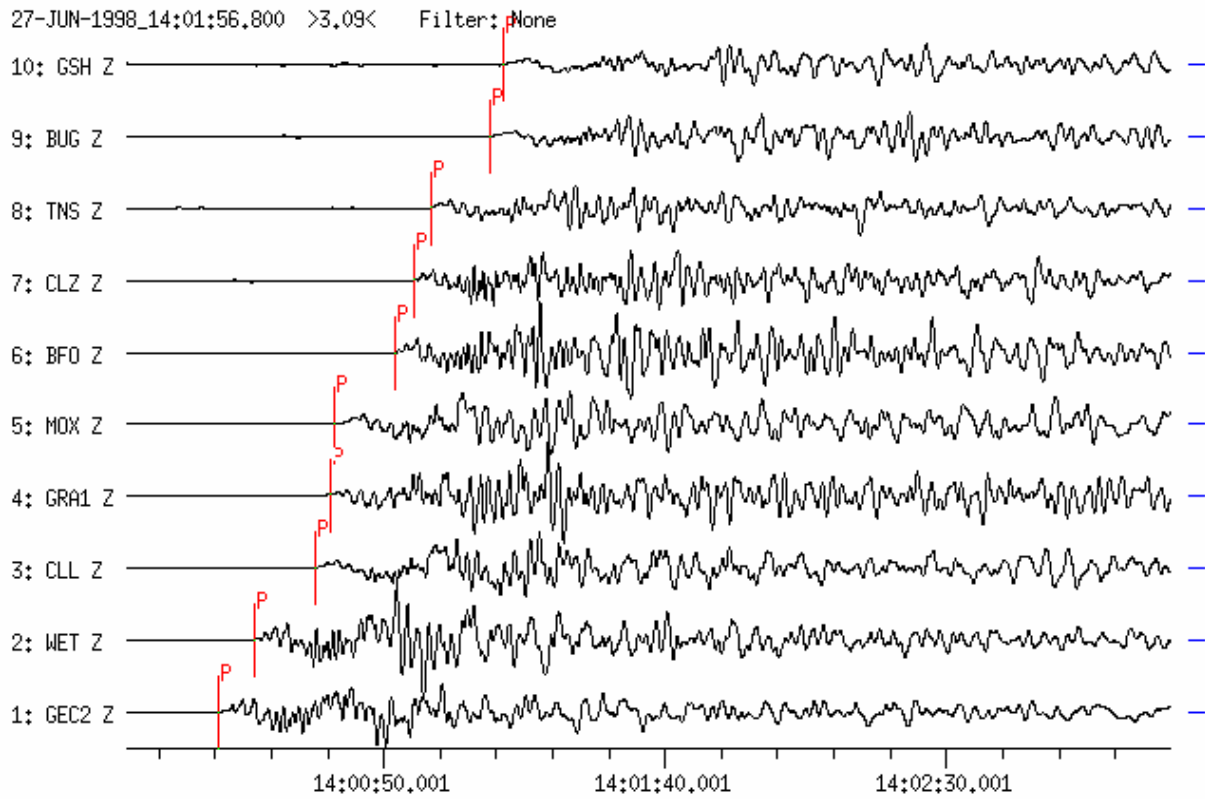


Figure 3a Broadband seismograms with high time resolution showing the complex P-wave groups. Records were made on vertical components of 10 GRSN stations at epicentral distances between $D = 19.7^\circ$ (GEC2) and 24.8° (GSH). Traces are sorted according to increasing distance. P waves on the individual traces are influenced by upper mantle discontinuities and signals are not coherent.

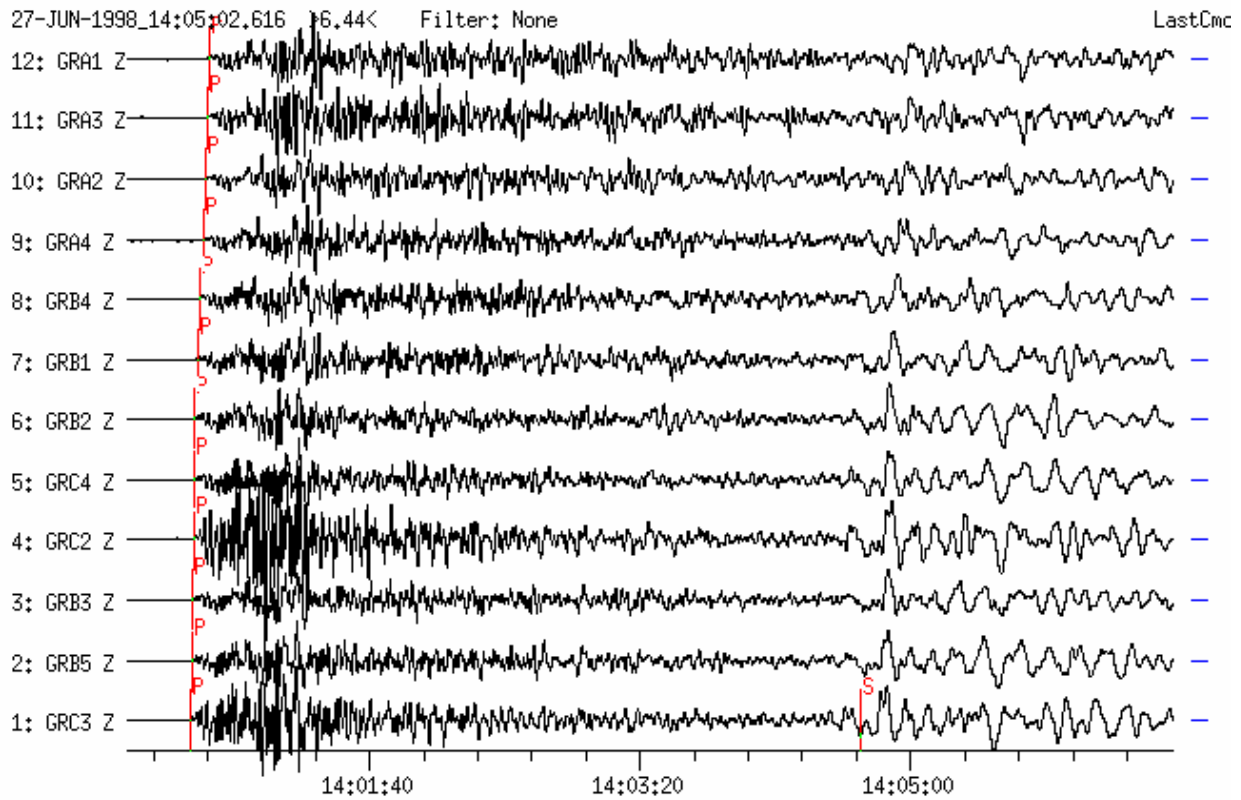


Figure 3b Broadband seismogram with P- and S-wave onsets recorded at 12 GRF-array stations. Traces are sorted according to increasing distance. P and S waves on the individual traces are influenced by upper mantle discontinuities and signals are also not coherent.

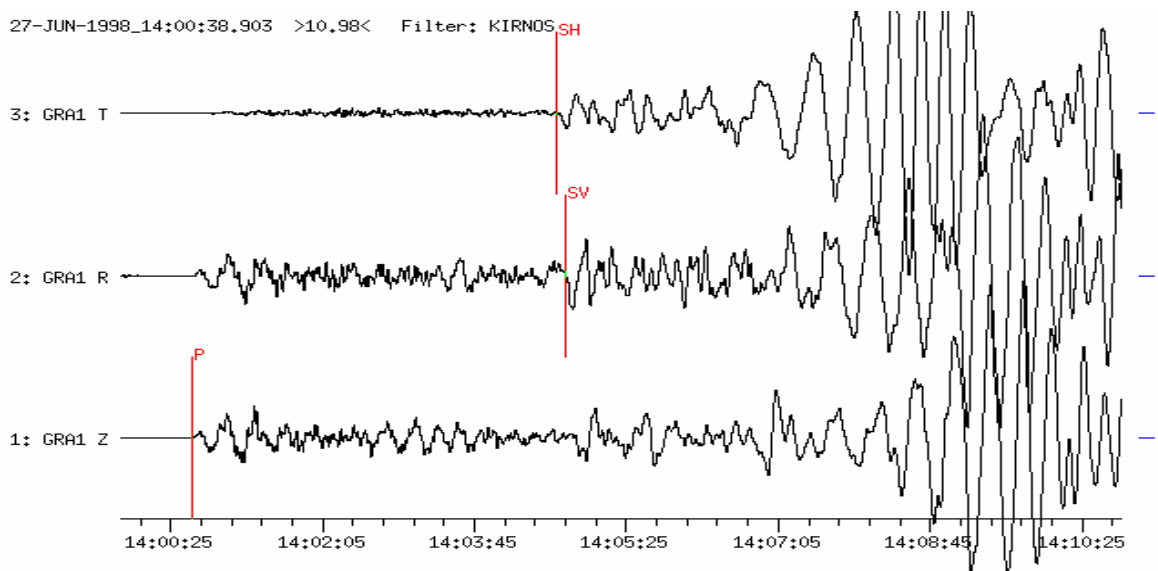


Figure 3c Three-component displacement-proportional KIRNOS-filtered seismogram recorded at the GRF-main-station GRA1 ($D = 21.6^\circ$). The original N- and E- horizontal components have been rotated with R showing into the source direction. The time difference between the onsets SH (horizontal polarized S wave) and SV (vertical polarized S wave) is about 4 sec. The reason for this difference may be the anisotropy of upper mantle layers.

Example 4: Earthquake in ICELAND REGION

USGS QED-data: 1998-06-04 OT 21:36:54.2 64.009N 21.294W h = 10G
 mb = 5.1 Ms = 5.1 (D = 22.5° to GRF)

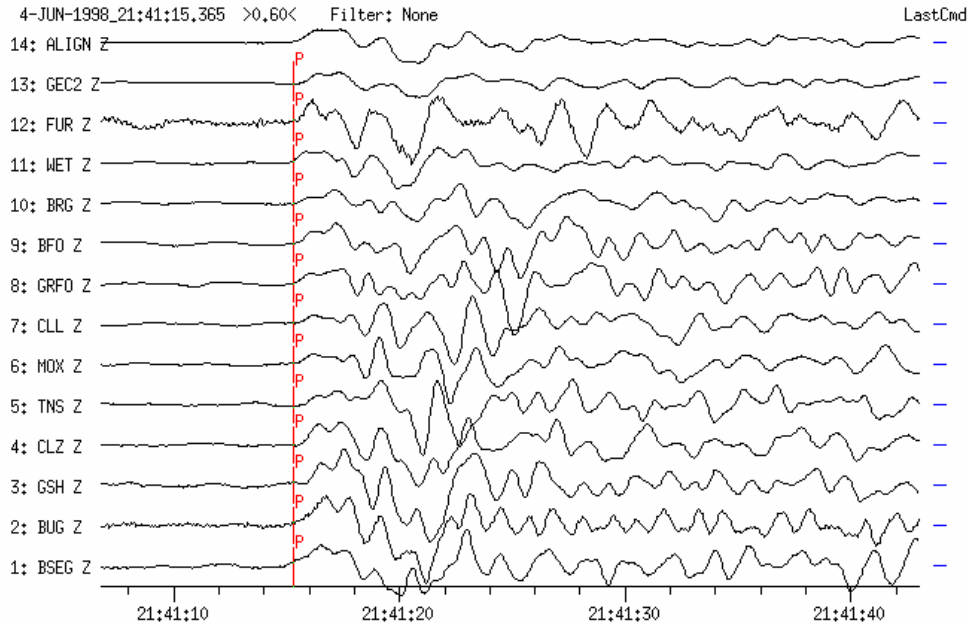


Figure 4a Broadband vertical-component seismograms recorded at 13 GRSN stations. Traces are sorted according to increasing epicentral distance ($D = 18.9^\circ$ to BSEG and 24.2° to GEC2), shifted in time and aligned for better signal comparison. All signals are incoherent and influenced by upper mantle discontinuities.

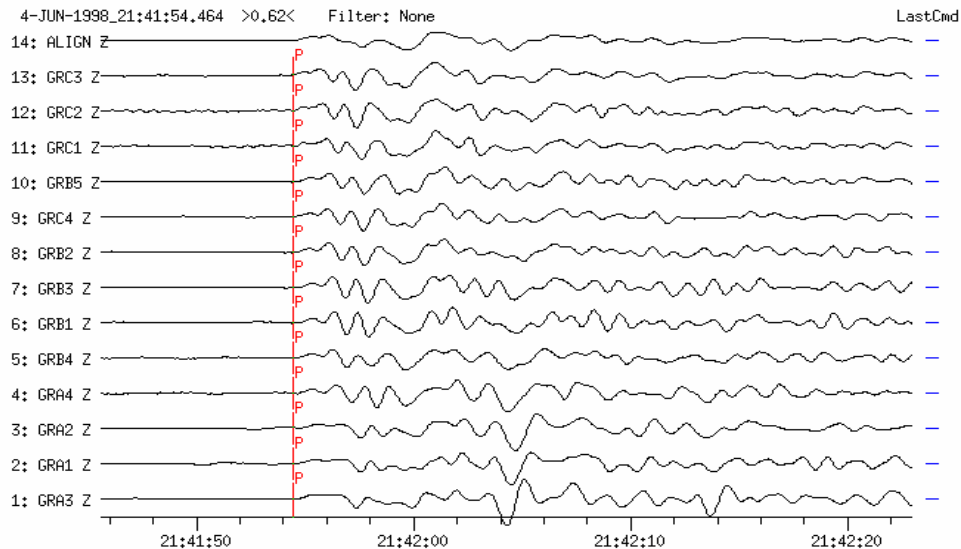


Figure 4b Broadband vertical-component seismograms recorded at the GRF-array stations. Traces are sorted according to increasing distance ($D = 22.48^\circ$ to GRA3 and 23.27° to GRC3), shifted in time and aligned for better signal comparison. Because of the smaller aperture of the array as compared to the GRSN network signals are more similar. At the nearest stations (GRA3 up to GRA4) a second onset appears about 10 s after P.

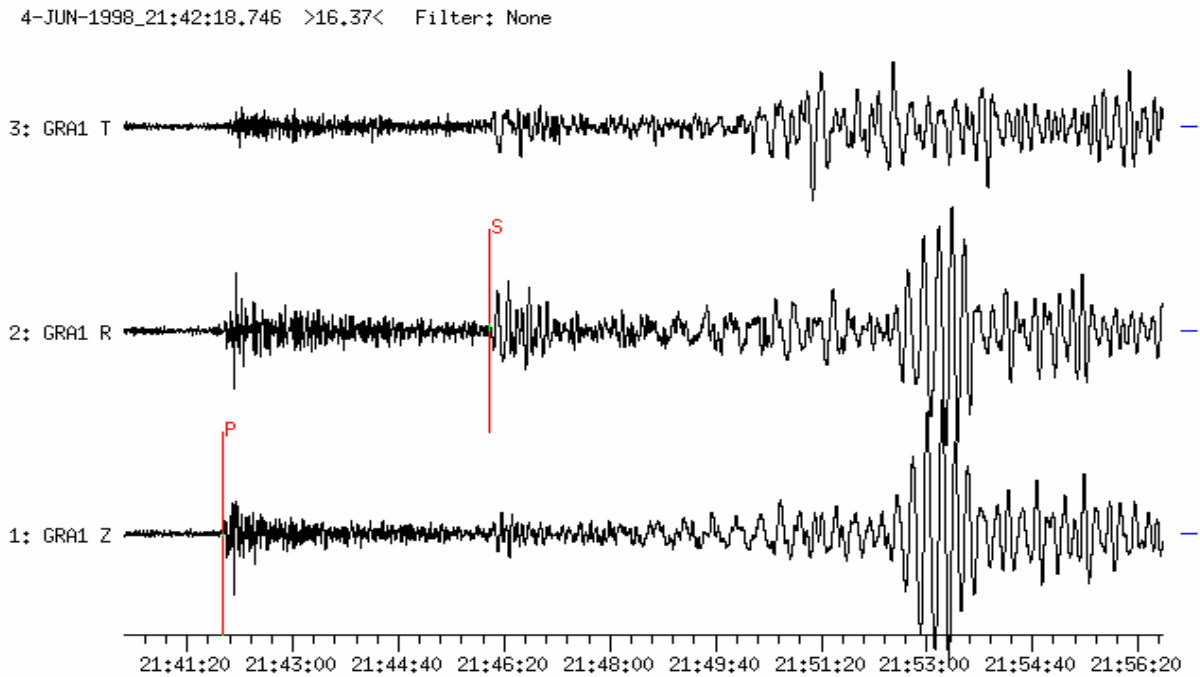


Figure 4c Simple three-component broadband seismogram at station GRA1 ($D = 22.5^\circ$) with clear P, S and surface waves. Horizontal components have been rotated (ZRT) with R into source direction.

Example 5: Earthquake at the Afghanistan -Tajikistan border region

USGS QED-data: 1998-05-30 OT 06:22:28.7 37.050N 70.086E h = 33N
 mb = 5.8 Ms = 6.9 ($D = 43.5^\circ$ and $BAZ = 83.7^\circ$ from GRF)

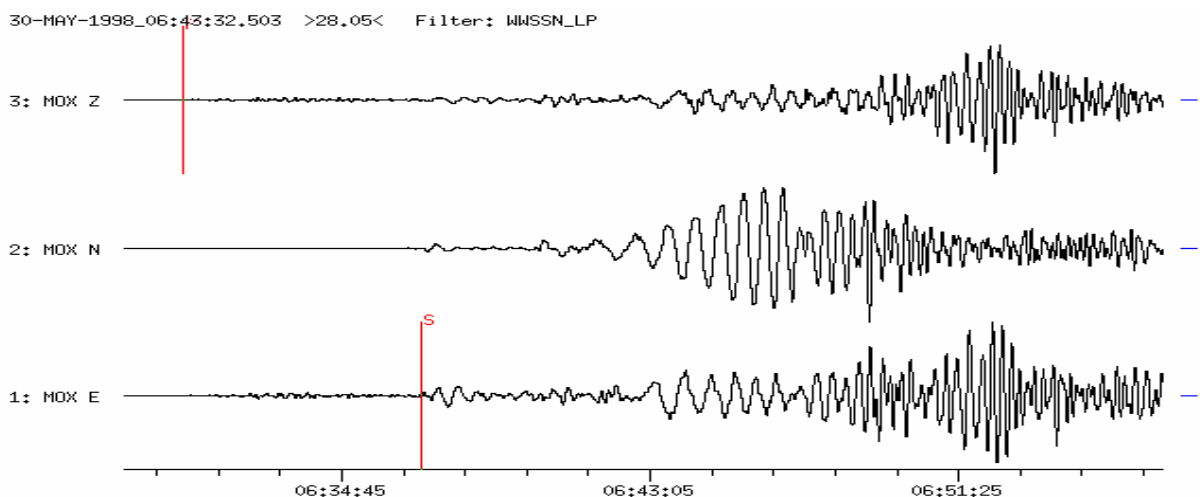


Figure 5a Three-component long-period seismogram (WWSSN-LP simulation filter) recorded at station MOX ($D = 43.2^\circ$, $BAZ = 85^\circ$) with P, S and dispersed surface waves. The nuclear explosion in Pakistan (see Figure 6.2) was recorded within the coda of this strong earthquake. As compared with the earthquake no surface waves has been recorded from the nuclear explosion.

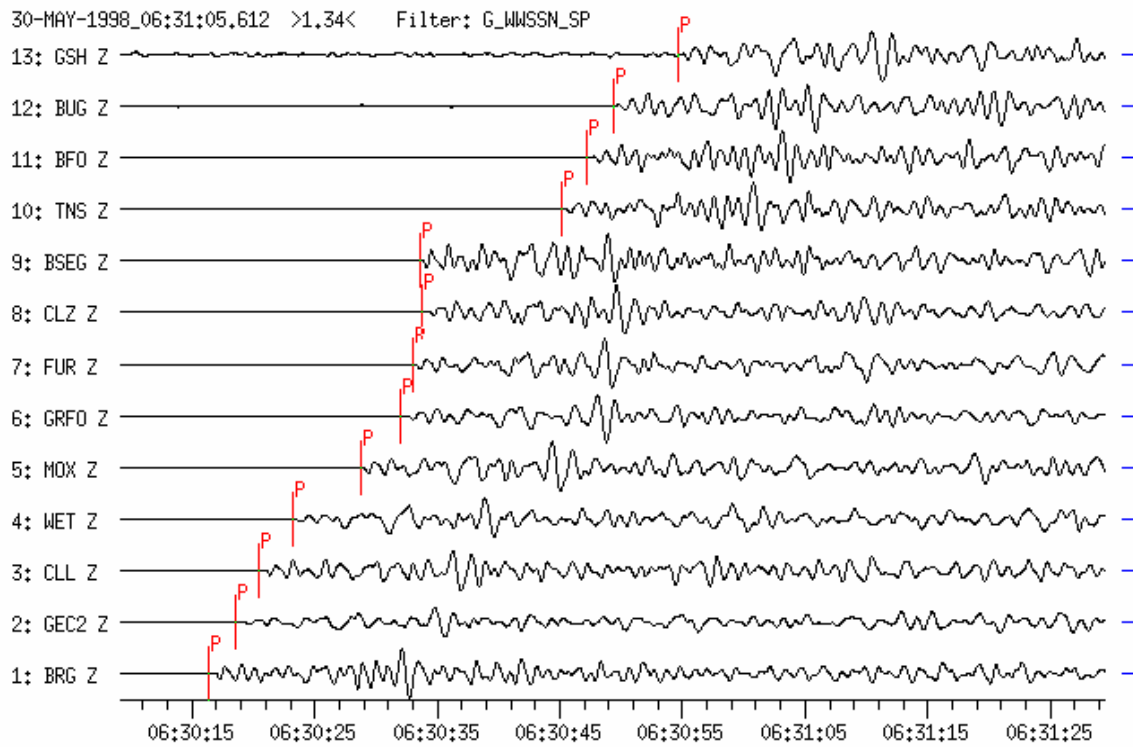


Figure 5b Short-period filtered P-wave onsets (WWSSN-SP simulation) recorded at 13 GRSN stations within the distance range between $D = 41.7^\circ$ (BRG) and 46.5° (GSH). P-wave trains are rather complex as compared with the records of the nearby underground nuclear explosions (see DS 11.4, Figures 2 and 3).

Example 6: Deep-focus earthquake in the HINDUKUSH REGION

USGS NEIC-data:1999-06-21 OT 17:37:29 36.40N 70.63E h = 249km
 mb = 5.7 (D = 44.3° to GRF, BAZ = 84.1 deg)

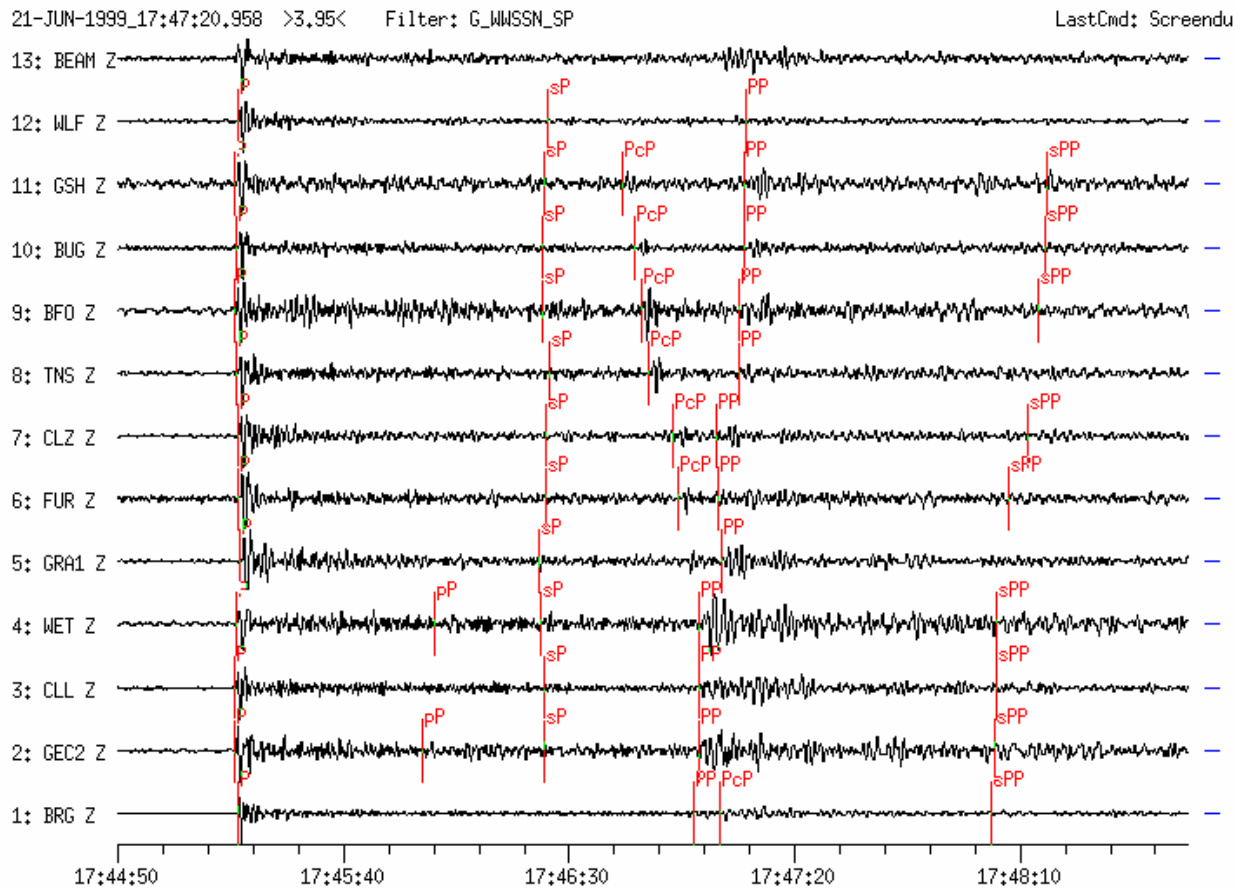


Figure 6a Short-period filtered seismogram (WWSSN-SP simulation) recorded at 12 GRSN, GRF(GRA1), GERESS and GEOFON stations. Traces are sorted according to distance (D = 42.4° to BRG and 47.6° to WLF), shifted and aligned for P onsets. Note that the travel-time curves for PcP and PP intersect in this distance range. Depth phases pP and sP (see the marked theoretically expected arrival times) are not visible on this short-period filtered record.

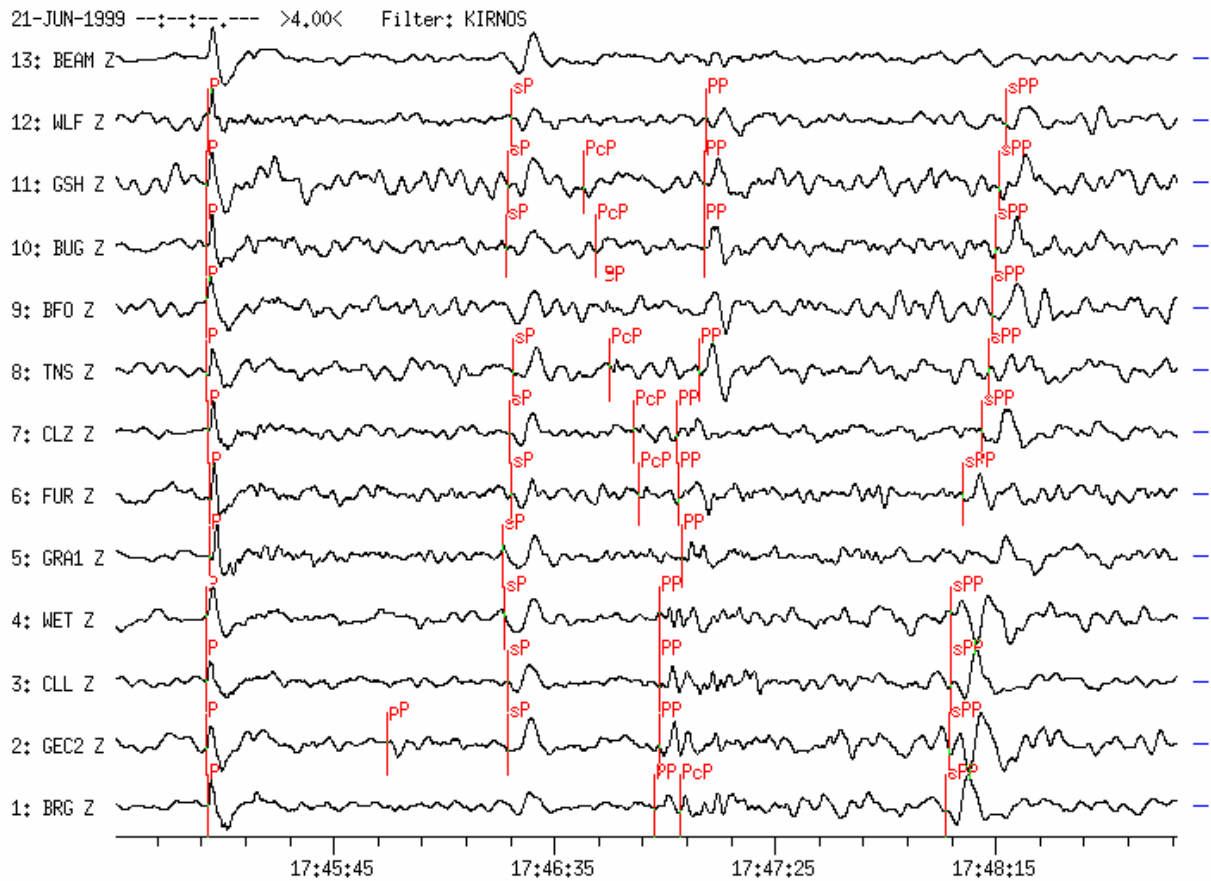


Figure 6b Stations and source parameter as in Figure 6a, however records of displacement-proportional Kirnos-simulation. Phases P, PP and the depth phases sP, sPP are clearly visible on these records while the phase pP is recognizable only at GEC2.

Example 7: Earthquake in the Laptev Sea Region

USGS NEIC-data: 1996-06-22 OT 16:47:13.1 75.812 N 134.710 E h = 10G
 mb = 5.6 Ms = 5.5

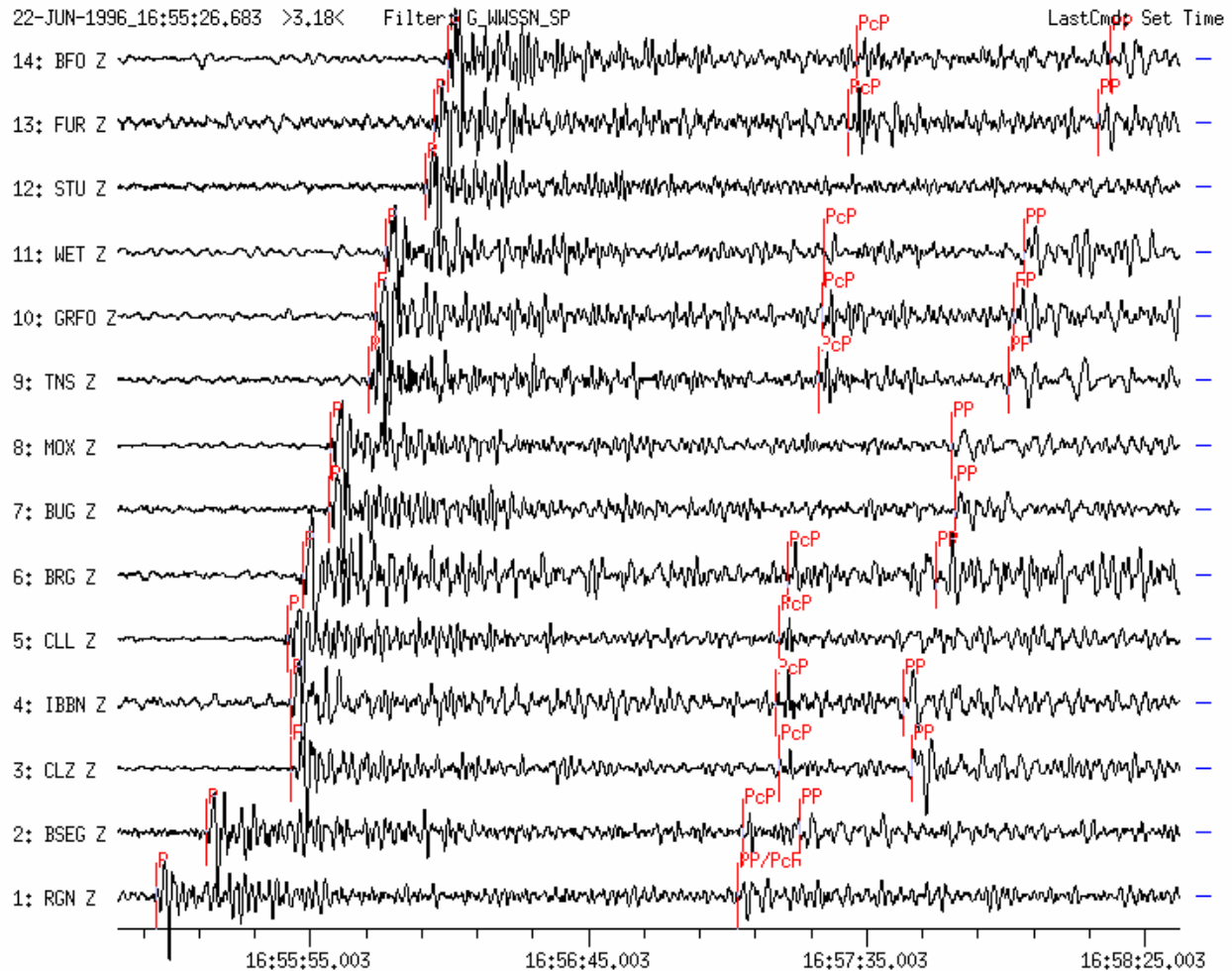


Figure 7a Vertical (Z) component short-period seismograms (WWSSN-SP simulation filter) recorded at 14 GRSN stations. Traces are sorted according to increasing epicentral distance which ranges between $D = 44.5^\circ$ for RGN (with $BAZ = 17.5^\circ$) and 51.4° for BFO (with $BAZ = 14.7^\circ$). P, PcP and PP are clearly visible. Note the decreasing travel-time difference (PcP - P) with increasing epicentral distance and the related small slowness values ($sl < 4$ s/deg) for the core-reflected wave PcP. At a distance of about 45° (see record of station RGN) the travel-time curves of PcP and PP intersect. Generally, PcP is well recorded on short-period filtered records, however no PcP onset is recognizable above the noise level in the records of stations STU, MOX and BUG.

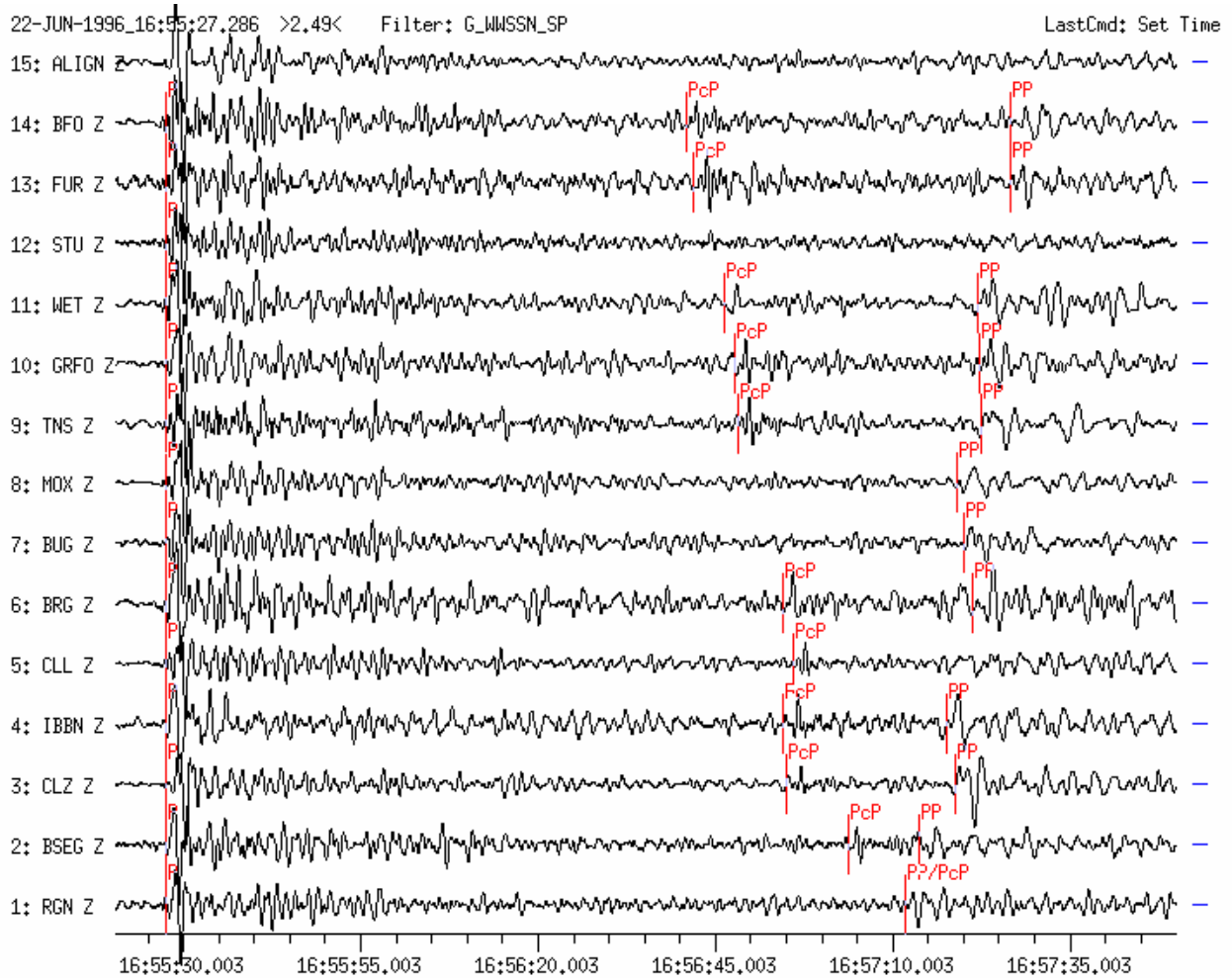


Figure 7b The same records as in Figure 7a, however, traces have been time-shifted and aligned for the P onsets. This figure shows more clearly the decreasing travel-time difference (PcP - P) with increasing distance from the epicenter.

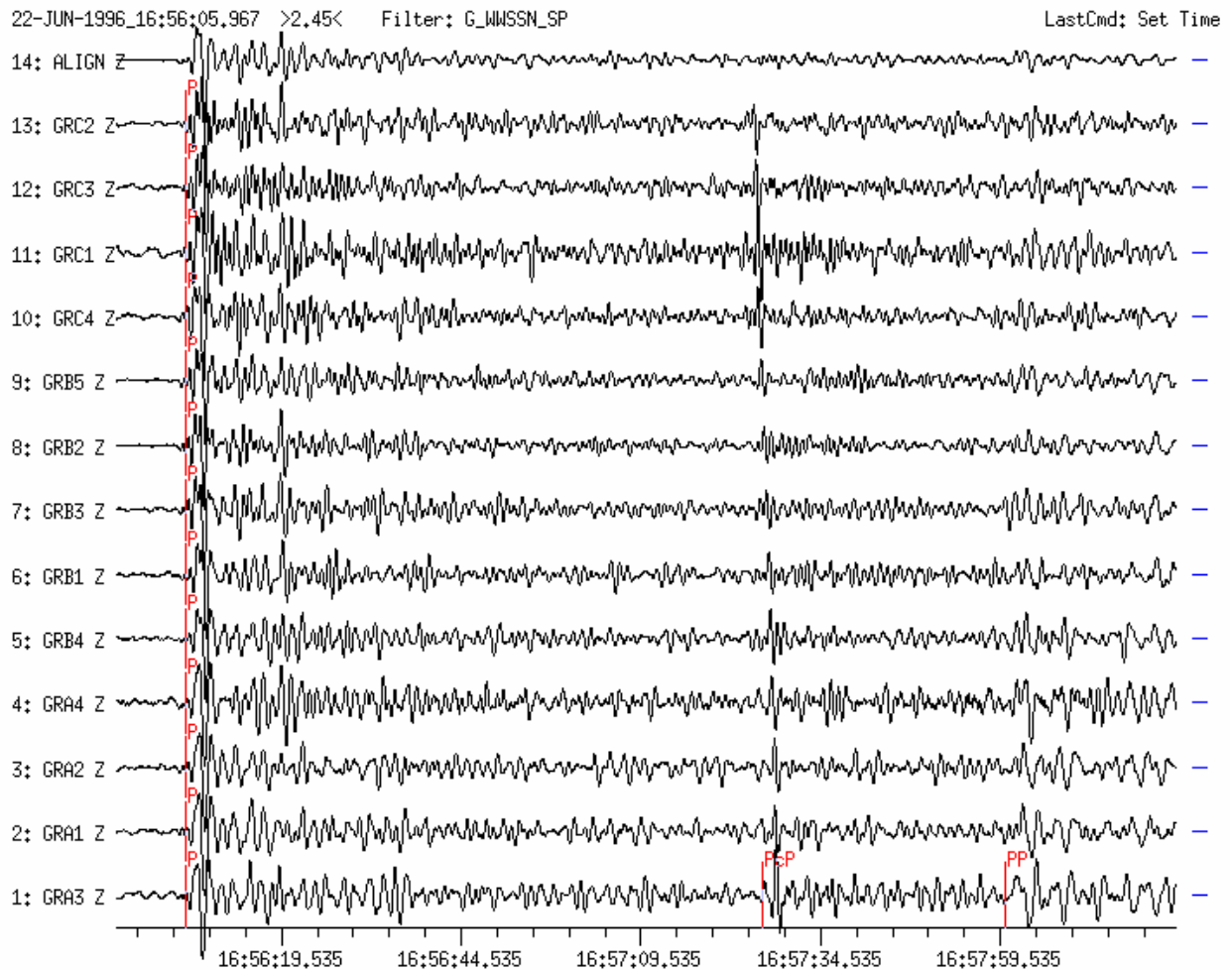


Figure 7c Short-period filtered seismograms recorded at the GRF-array. Traces are sorted according to increasing distance ($D = 49.48^\circ$ to GRA3 and 50.33° to GRC2), shifted in time and aligned for P onsets. Phases P, PcP and PP have been marked. Because of the smaller spacing of the array-stations as compared with the GRSN stations, the decrease of the travel-time difference PcP-P is less obvious.

Example 8: Record of an earthquake in Mongolia

USGS-QED-data: 1998-09-24 OT 18:53:40.2 46.274 N 106.237 E h = 33km
 mb = 5.3 Ms = 5.4, (D = 59.4° and BAZ = 54° from GRF(GRA1))

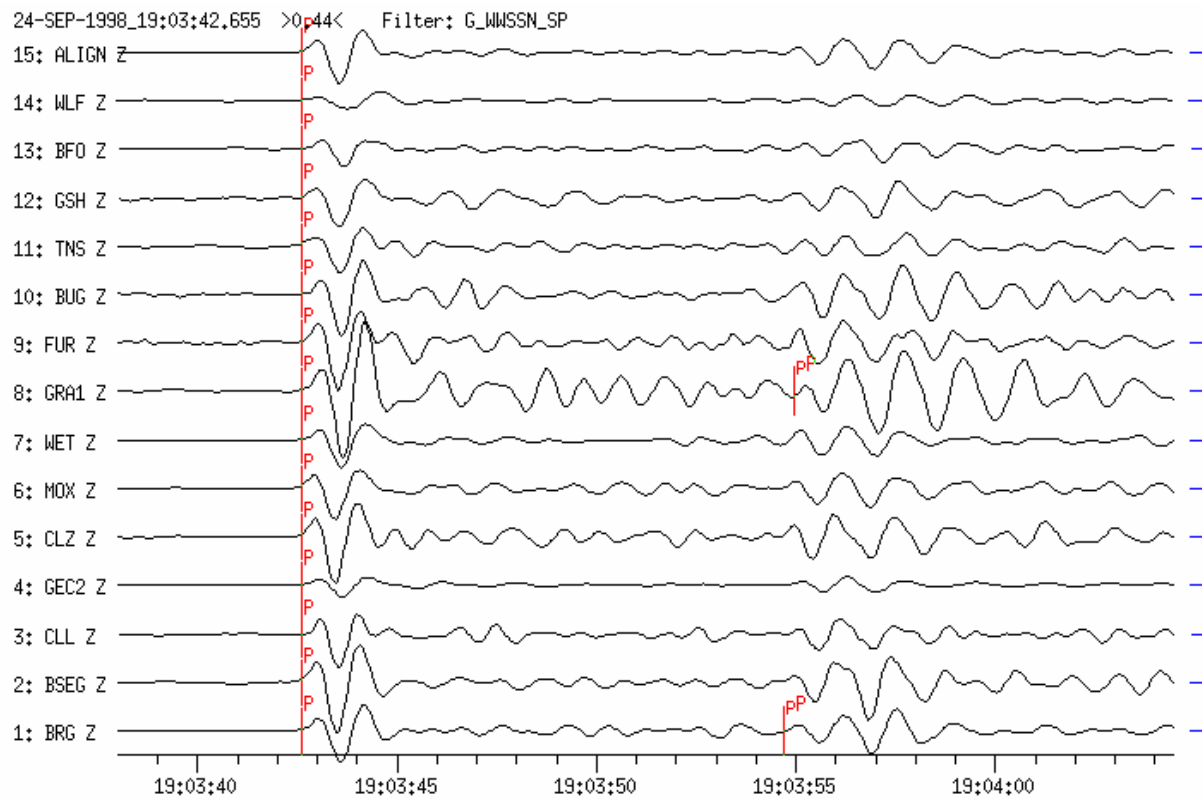


Figure 8a This is an example for an event with coherent short-period P waves within the GRSN (WWSSN-SP simulation filter). Additionally, the record of the GEOFON-station WLF in Luxembourg is shown on trace No.14. The traces are sorted according to increasing distance (D = 57.3° to BRG and 62.1° to WLF), shifted and aligned for P onsets. The most remarkable feature is the strong variability of the P-wave signal-amplitudes within this regional network. The table below gives the measured amplitudes together with the calculated magnitudes. Body-wave magnitudes mb vary between 5.4 (GEC2) and 6.2 (GRA1). The depth phase pP was used to estimate a better source depth (h = 44 km) than the value given in the QED (h = 33 km).

Table 8a Result of the seismogram analysis shown in Figure 8a. The table was printed from the GRSN databank and contains in the uppermost line source parameters like date, an event identification number (ev_id) and the name of the analyst (KLI for Klinge). The following lines give the analyzed stations, onset times, phases, polarities, components, periods T, maximum amplitudes A, body- and/or surface-wave magnitudes mb/MS, epicentral distances D, beam-slowness b_slo, beam_azimuths b_az. The lowermost part of the table contains source parameters like analysis center (SZGRF), origin time OT, latitude, longitude, average magnitude values for mb and MS, depth of the source and source region. Note the significant differences between the magnitude estimates mb from records of different network stations.

						ev_id 980924007	KLI
1998-09-24							
BRG	19:03:27.2	e P	Z	T 1.2	A 135.5	mb 5.9 D 58.3	
ALIGN	19:03:27.2	e P	Z	T 1.1	A 124.1	mb 5.8	
BSEG	19:03:28.2	e P	Z	T 1.1	A 198.3	mb 6.0 D 58.4	
CLL	19:03:28.6	e P	Z	T 0.9	A 98.9	mb 5.8 D 58.5	
GEC2	19:03:36.3	i P	c Z	T 1.2	A 46.9	mb 5.4 D 59.6	
CLZ	19:03:36.6	e P	Z	T 1.1	A 177.7	mb 6.0 D 59.6	
MOX	19:03:36.9	e P	Z	T 1.2	A 122.4	mb 5.8 D 59.6	
WET	19:03:38.5	e P	Z	T 1.2	A 107.2	mb 5.7 D 59.9	
BRG	19:03:39.3	e pP	Z				
GRA1	19:03:42.6	i P	c Z	T 1.1	A 286.5	mb 6.2 D 60.4	
					b_slo 6.8	b_az 54	
BUG	19:03:48.5	e P	Z	T 1.1	A 162.4	mb 5.8 D 61.4	
FUR	19:03:48.6	e P	Z	T 1.1	A 174.3	mb 5.8 D 61.3	
TNS	19:03:49.9	e P	Z	T 1.1	A 103.0	mb 6.0 D 61.5	
GSH	19:03:54.5	e P	Z	T 1.3	A 132.3	mb 6.0 D 62.3	
GRA1	19:03:55.0	e pP	Z				
BFO	19:03:57.4	e P	Z	T 1.1	A 55.2	mb 5.6 D 62.8	
WLF	19:04:00.1	e P	Z	T 1.7	A 80.3	mb 5.6 D 63.0	
GRA1	19:11:52.2	e S	E			D 60.4	
GEC2	19:30:36.0	e L	Z	T 19.9	A 3895.8	MS 5.5	
GRA1	19:31:03.6	e L	Z	T 20.6	A 3398.7	MS 5.5	
SZGRF	OT 18:53:39.3	45.30N	106.84E		mb_av 5.8	MS_av 5.5	
DEP	44km	▲ MONGOLIA					

Example 9: Earthquake in California

SZGRF-data:1999-10-16 OT 09:46:55 34.9N 115.9 W mb = 6.6 Ms = 7.9
 The event happened east of Los Angeles (D = 83.6° BAZ = 319° from GRF) .

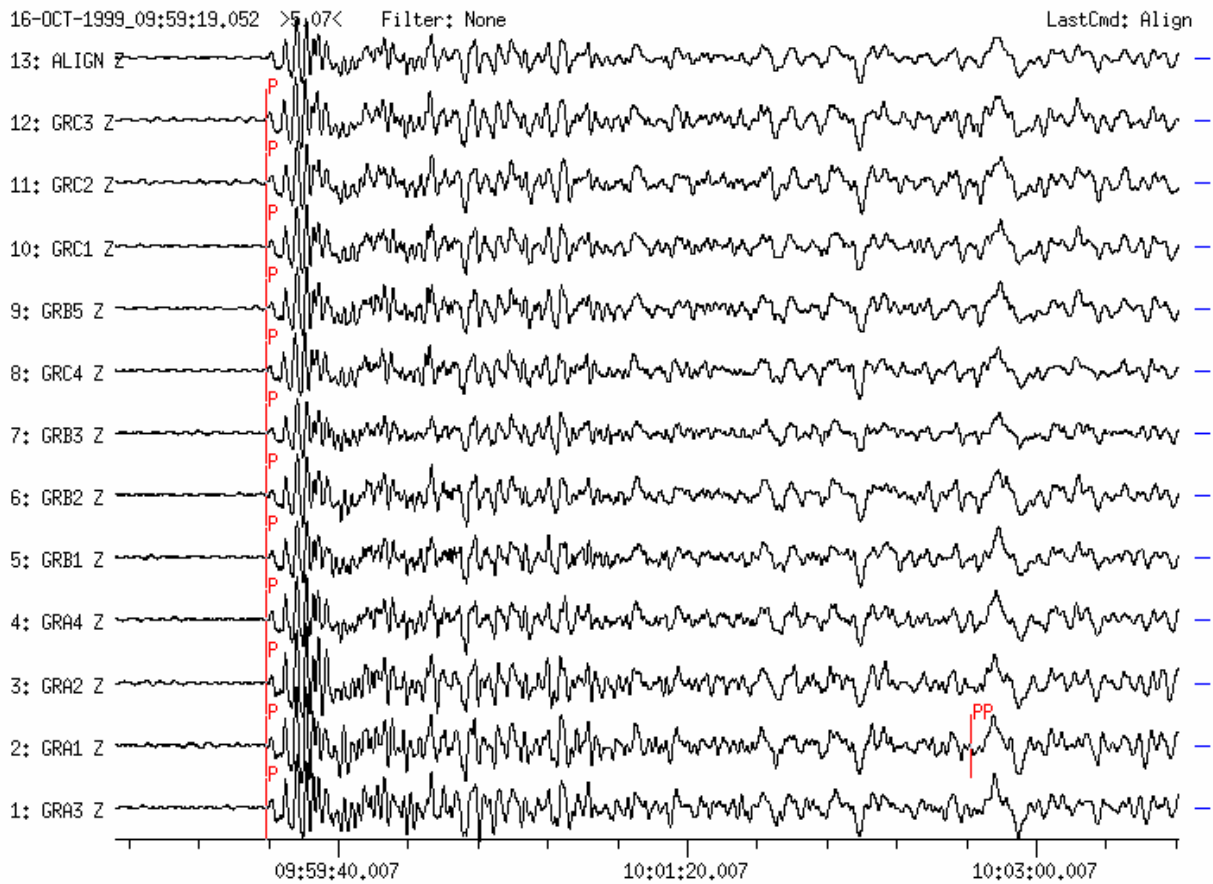


Figure 9a Broadband vertical-component seismograms recorded at 12 GRF-array stations. Traces are sorted according to increasing distance (D = 83.6° to GRA3 and 84.4° to GRC3), shifted in time and aligned for P onsets. The coherent phases P and PP are marked, however some more onsets appear ahead of PP.

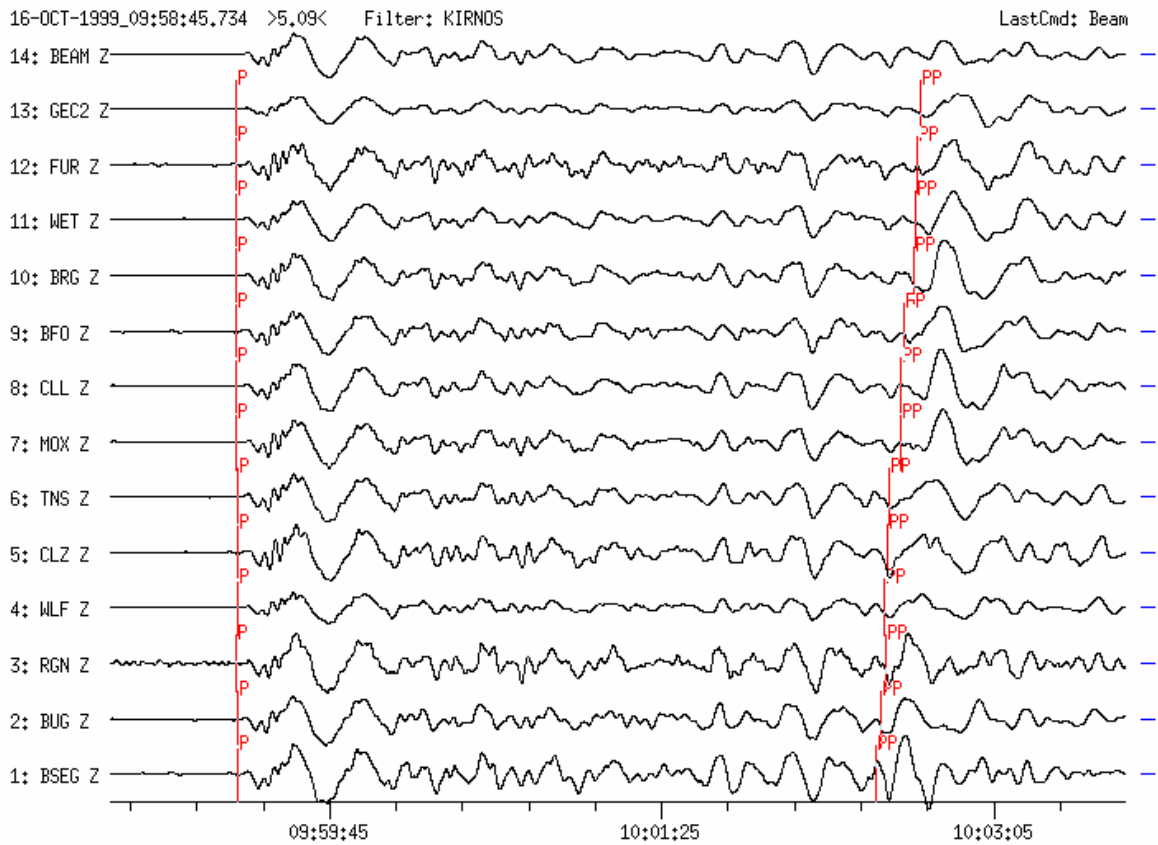


Figure 9b Broadband vertical-component seismograms recorded at 13 GRSN-stations. Traces are filtered (Kirnos-simulation), sorted according to increasing distance (80.1° to BSEG and 85.3° to GEC2), shifted in time and aligned for P onsets. The used displacement proportional broad-band filter displays clearly the coherent part of the wave train from the network. As in Figure 9a, coherent phases appear ahead of PP that have slowness values as P.

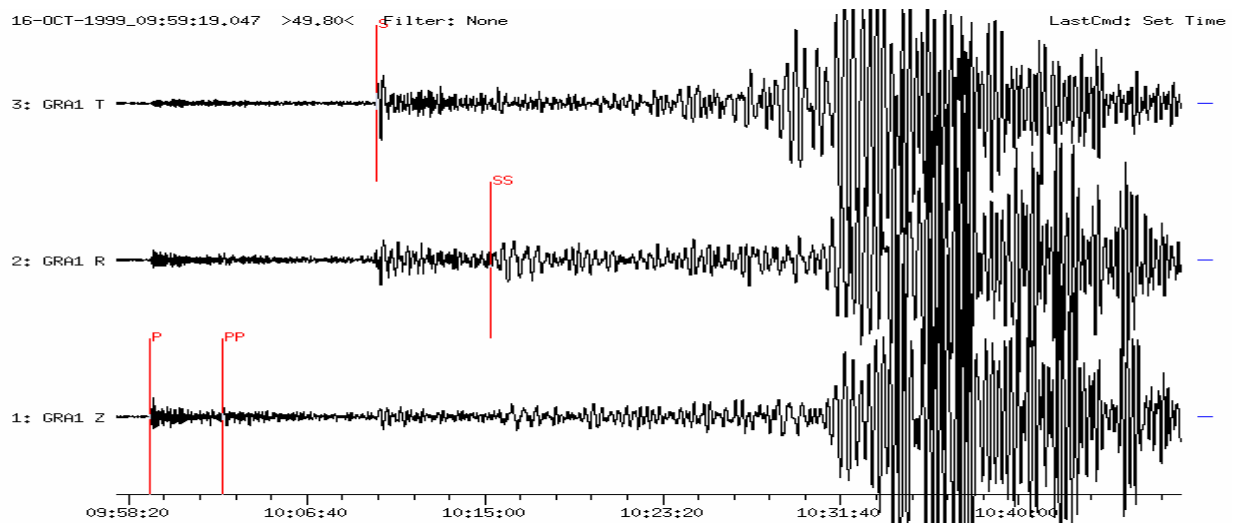


Figure 9c Broadband three-component seismogram recorded at GRA1 ($D = 83.6^\circ$). The horizontal components are rotated into the R and T direction. Phases P, PP, S, SS and surface waves are displayed. Rayleigh waves recorded on radial and vertical components appear later than Love waves recorded on the transversal component only.

Example 10: Earthquake near the coast of NICARAGUA

USGS NEIC-data: 1998-10-09 OT 11:54:29.0 11.337N 86.429W h = 10km
 mb = 5.6 Ms = 5.6 (D = 86.3° and BAZ = 282° from GRF(GRA1))

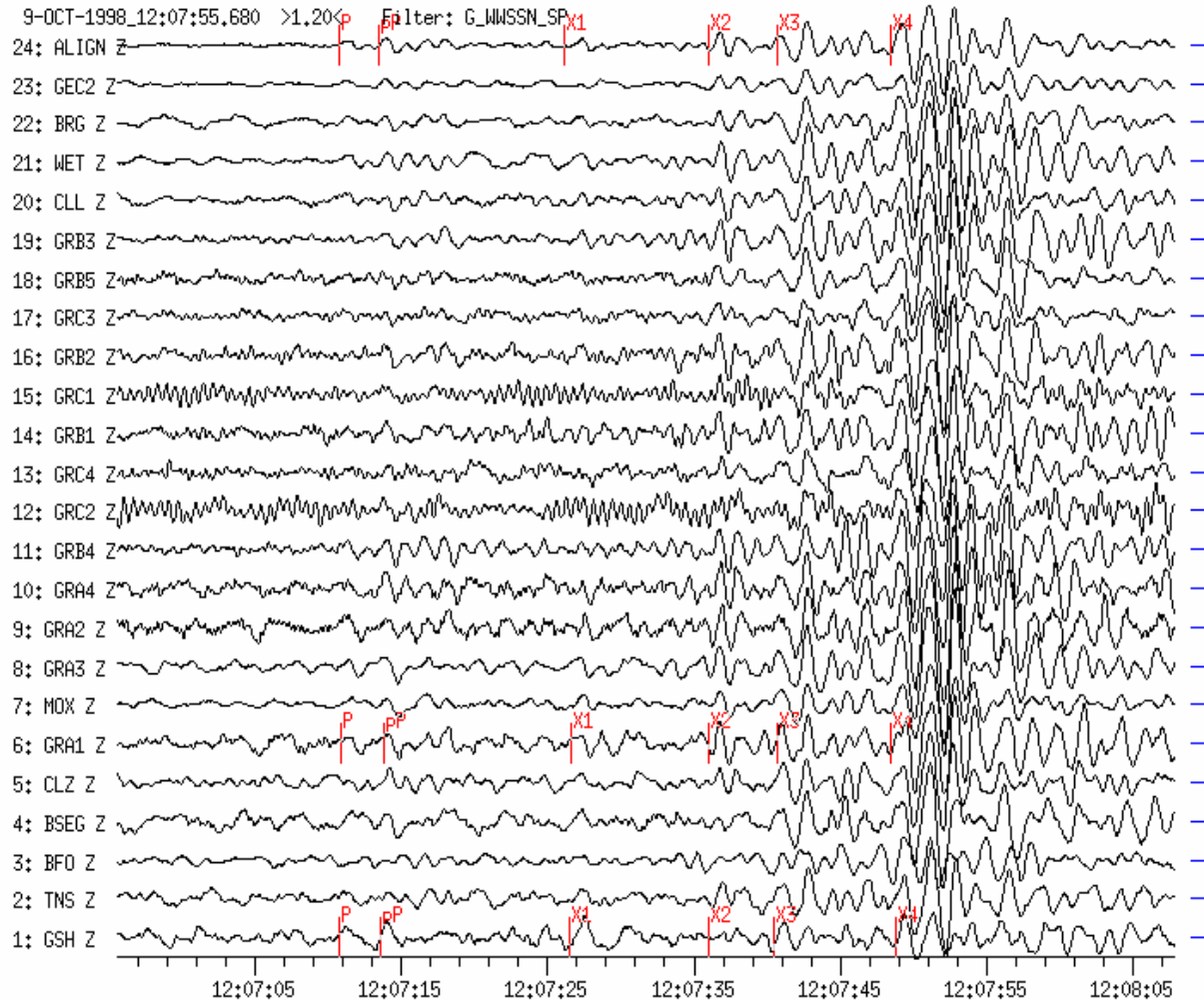


Figure 10a Short-period seismograms (WWSSN-SP simulation filter) from 23 broadband stations of the GRF-array, the GRSN network and the GERESS array (GEC2). Traces are time-shifted, aligned for P and sorted according to increasing distance (D = 83.1° to GSH and 88.1° to GEC2). Note the large number of onsets within the first 40 sec of the P-wave group (P, pP, X1, X2, X3, X4). The reason for these multiple onsets may be a multiple rupture process or (in some cases) reflections from the nearby subduction zone.

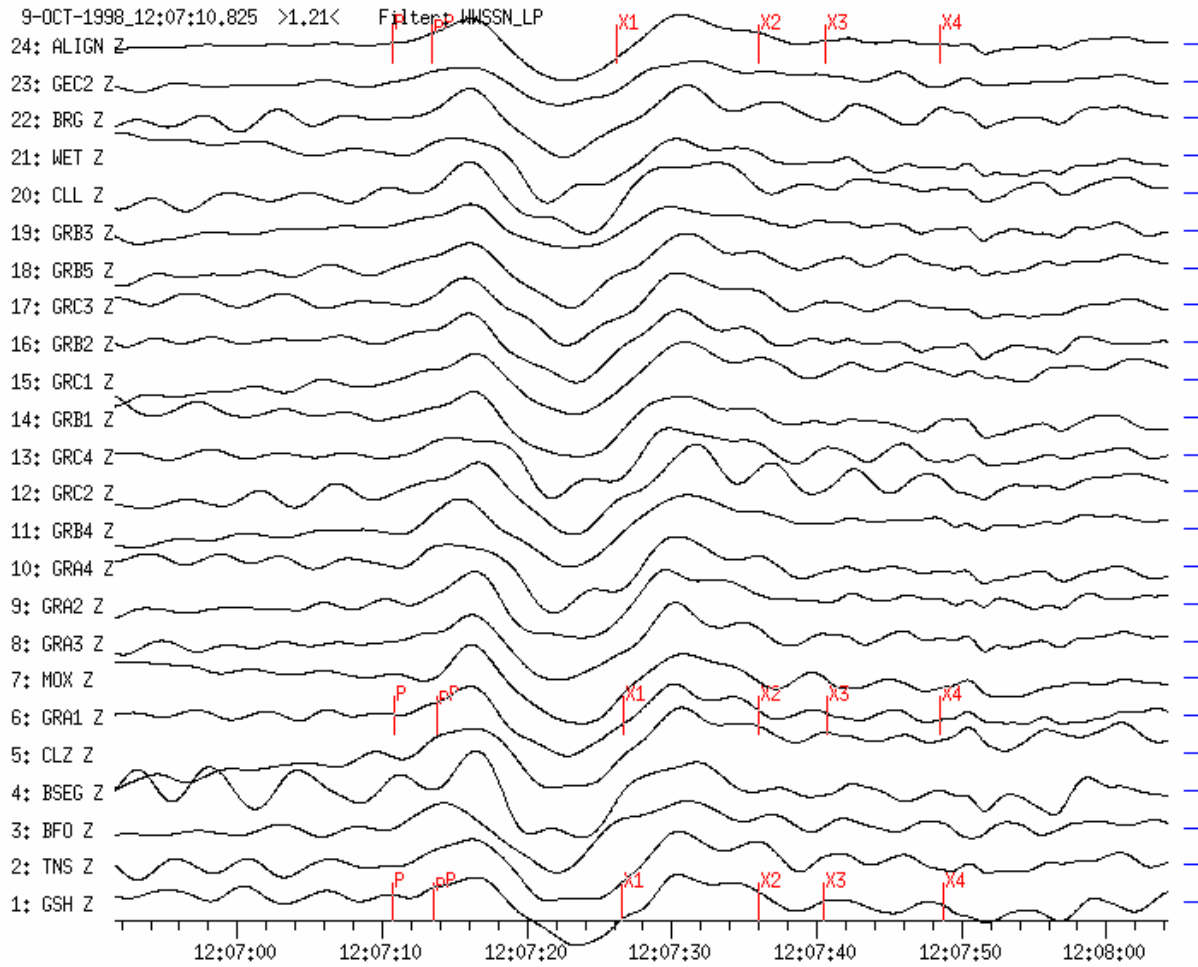


Figure 10b Long-period seismograms (WWSSN-LP simulation filter) of the same stations as in Figure 10a, depicted with high time-resolution. Traces are aligned and sorted according to increasing distance. Note the very long-period P-wave onset ($T \approx 14$ s) in the time window between P and X2 where the P-wave amplitudes are relatively small in the short-period filtered records whereas at X4, which is by far the largest onset in Figure 10a, no long-period wave onset is to be seen. This seems to speak of an initially “slow” earthquake rupture which then escalated into a faster rupture or the break of a “harder” asperity which generated more short-period energy.

9-OCT-1998_12:06:59.015 >45.21< Filter: SRO_LP

LastCmd: Theo (Table

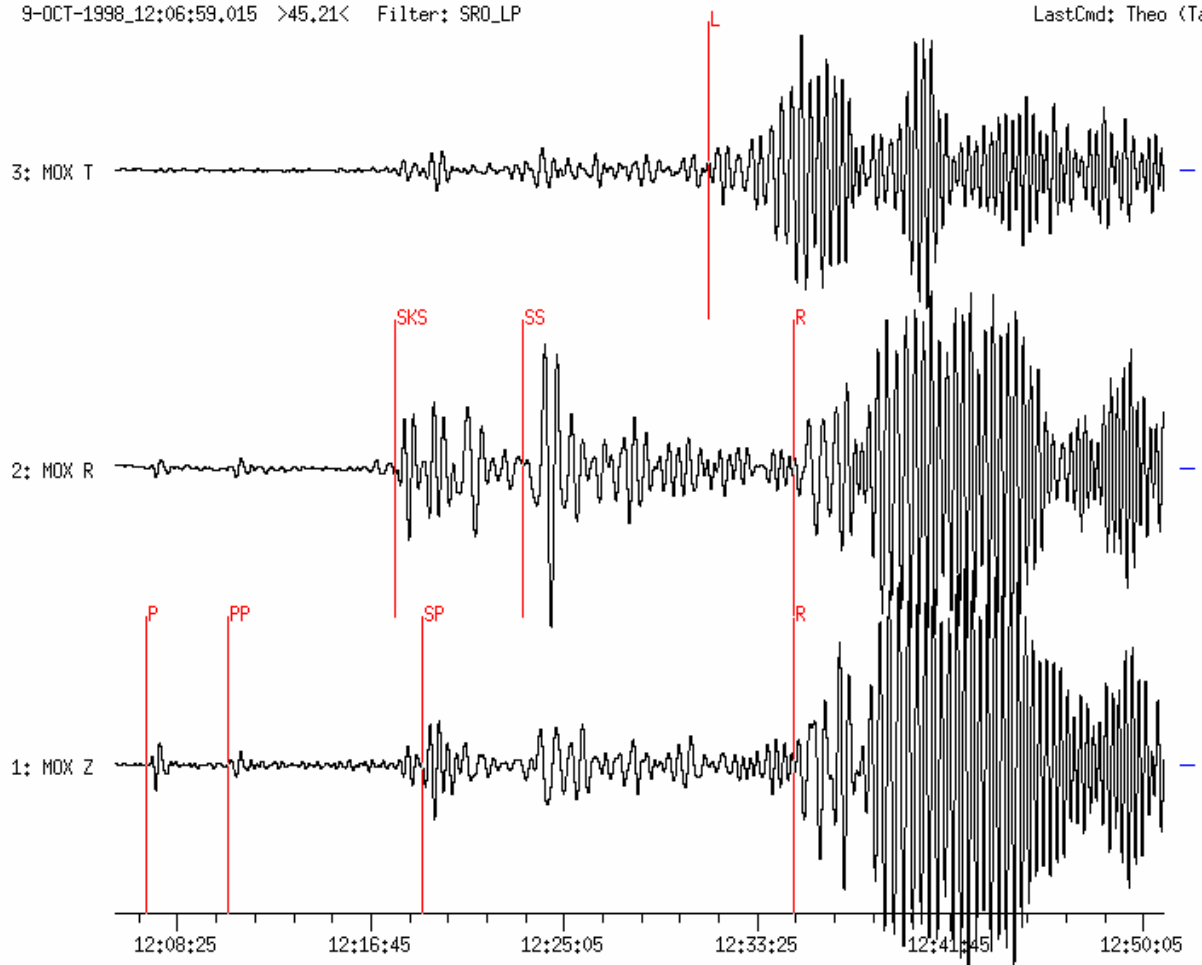


Figure 10c Time-compressed long-period filtered three-component seismogram (SRO-LP simulation filter) of the Nicaragua earthquake recorded at station MOX ($D = 86.4^\circ$, $BAZ = 283^\circ$). Horizontal components have been rotated into the R (radial) and T (transverse) direction. The seismogram shows long-period phases P, PP, SKS, SP, SS and surface waves L (or LQ for Love wave) and R (or LR for Rayleigh wave). Note the remarkably simple waveforms of P and PP as compared with the complicated structure in the short-period P-wave group in Figure 10a.

Example 11: Earthquake in Taiwan Region

USGS NEIC-data: 1996-08-10 OT 06:23:08 24.032 N 122.550 E h = 46G
 mb = 5.2 Ms = 5.2 (D = 87.1° and BAZ = 56.6° from BFO)

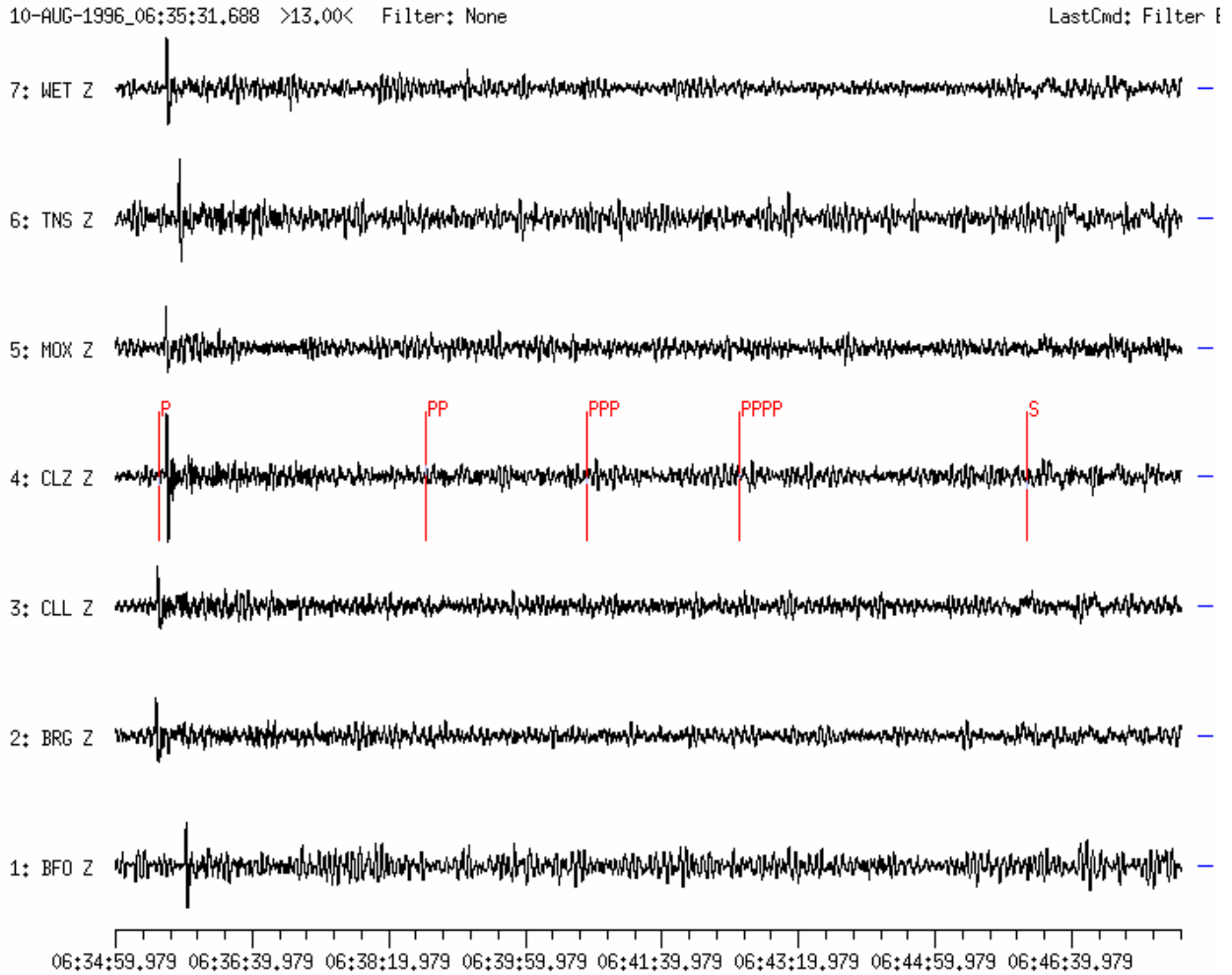


Figure 11a Broadband vertical-component seismograms of the Taiwan earthquake recorded at 7 GRSN-stations within the distance range $D = 82.9^\circ$ and 87.1° . Only the P-wave onset is recognizable on the records. Secondary onsets such as surface reflections of the P and S wave (theoretical onset times marked on the CLZ trace) are not to be seen above the noise level.

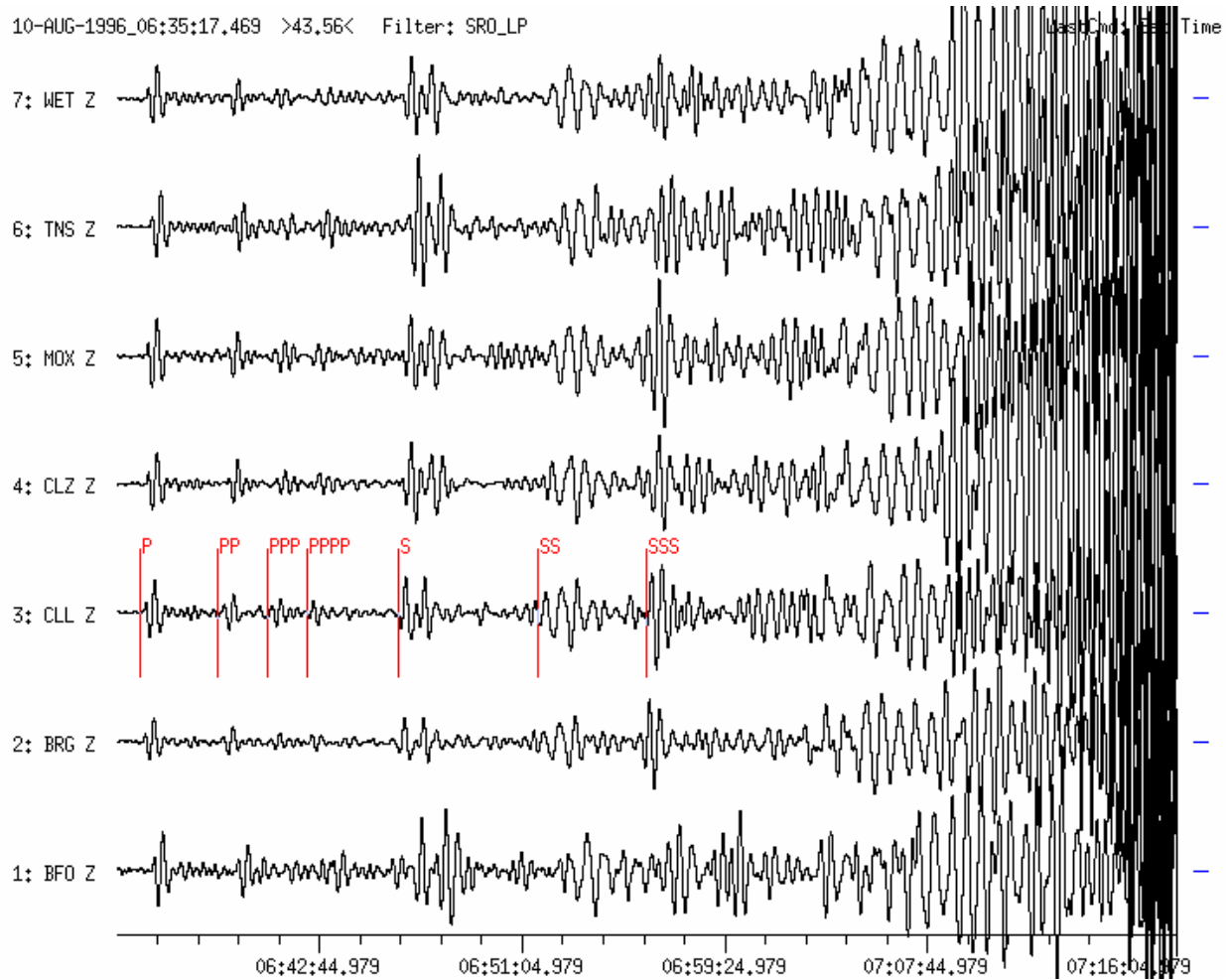


Figure 11b The same event as in Figure 11a after long-period filtering (SRO-LP simulation filter). Note the pronounced onsets of PP, PPP, PPPP as well as S, SS and SSS which are marked at the record trace of station CLL ($D = 82.9^\circ$). Phase identification is eased by using absolute (see overlay to Fig. 2.48) or differential theoretical travel-time curves (see Figure 4 in Exercise EX 11.2). This is essential when interpreting single station recordings. Modern seismogram analysis program can automatically mark the theoretically expected onset times of the various phases when the epicentral distance to the station and the source depth are known or assumed. When a network of stations or array is available, phase identification is supported by *vespagram* analysis as shown in the following figure.

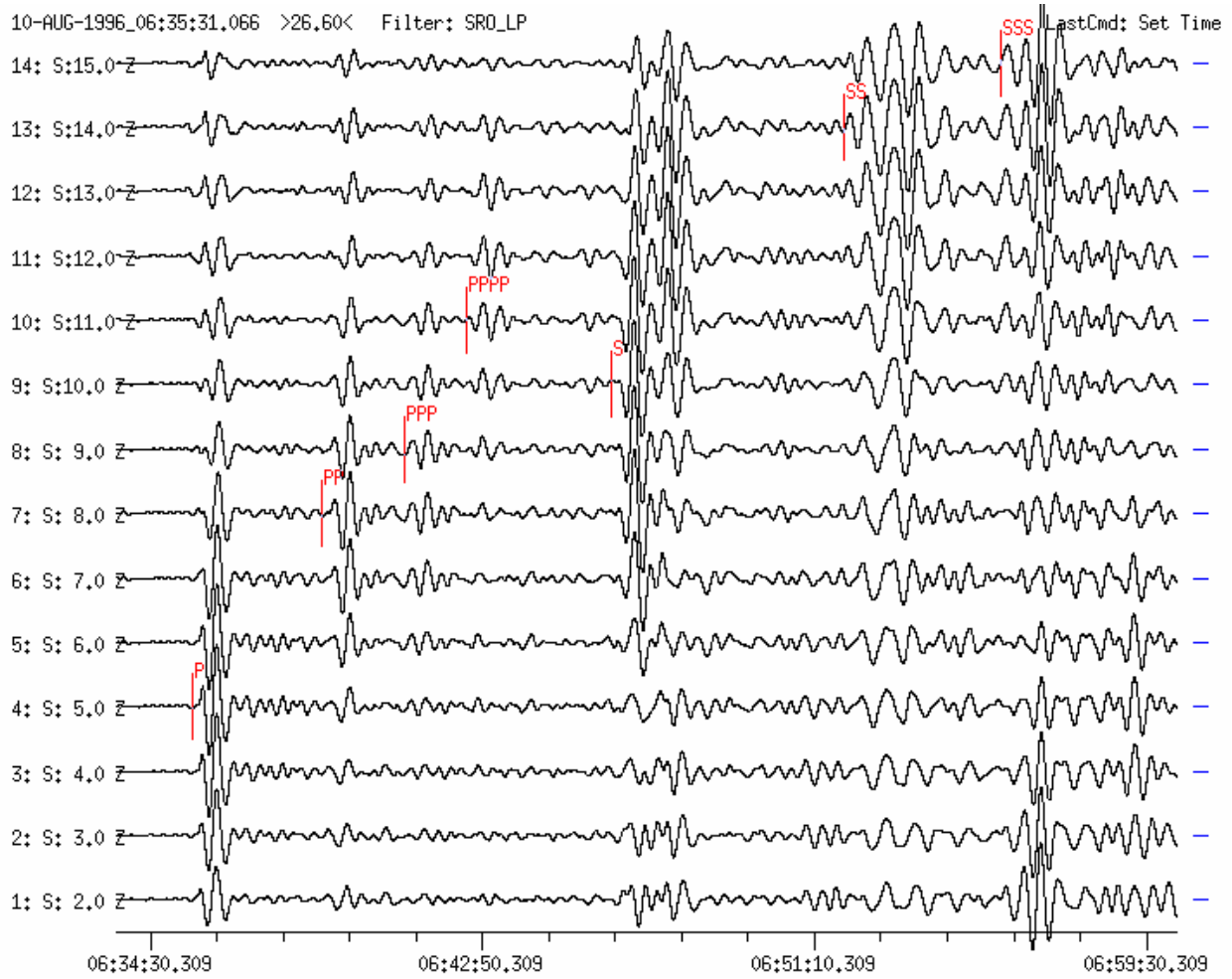


Figure 11c For better phase identification a [vespagram analysis](#) (see 9.7.7 in Chapter 9) of the long-period filtered traces was made. Identified phases have been marked on their respective slowness trace S (e.g., P on trace 4 with slowness $S = 5.0 \text{ s}^\circ$ and PP on trace 7 with $S = 8.0 \text{ s}^\circ$). In the vespagram traces the respective phases have the largest amplitudes at their proper slowness value.

Example 12: Earthquake in the region of Michoacan, Mexico

USGS NEIC-data: 1997-01-11 OT 20:28:26.0 18.193 N 102.800 W h = 33G
 mb = 6.5 Ms = 6.9 (D = 90.9° and BAZ = 299.7° from GRFO site)

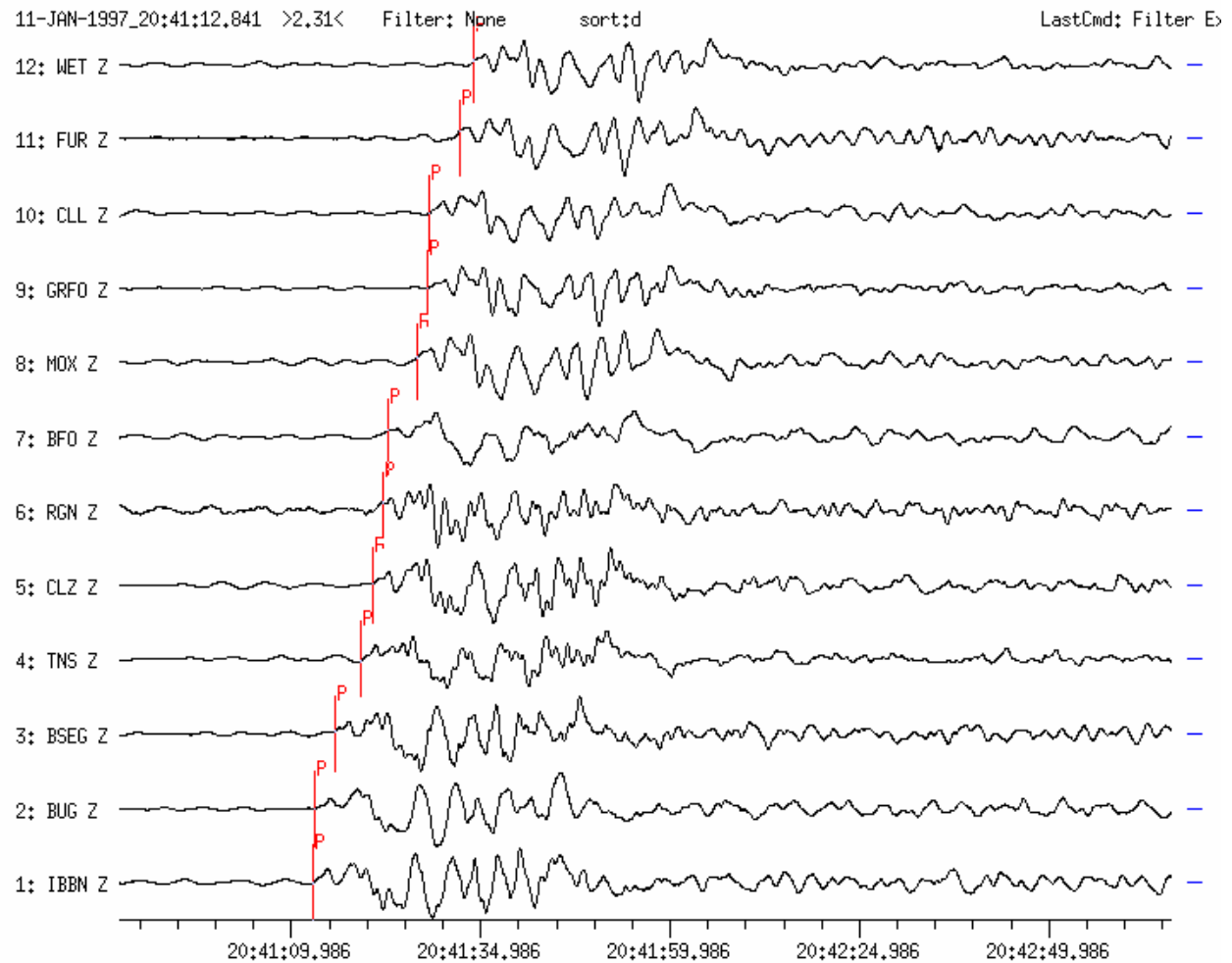


Figure 12a Broadband vertical-component seismograms recorded at 12 GRSN-stations are shown. Traces are sorted according to increasing distance of the stations (D = 87.7° to IBBN and 92.1° to WET). P-wave onsets are marked.

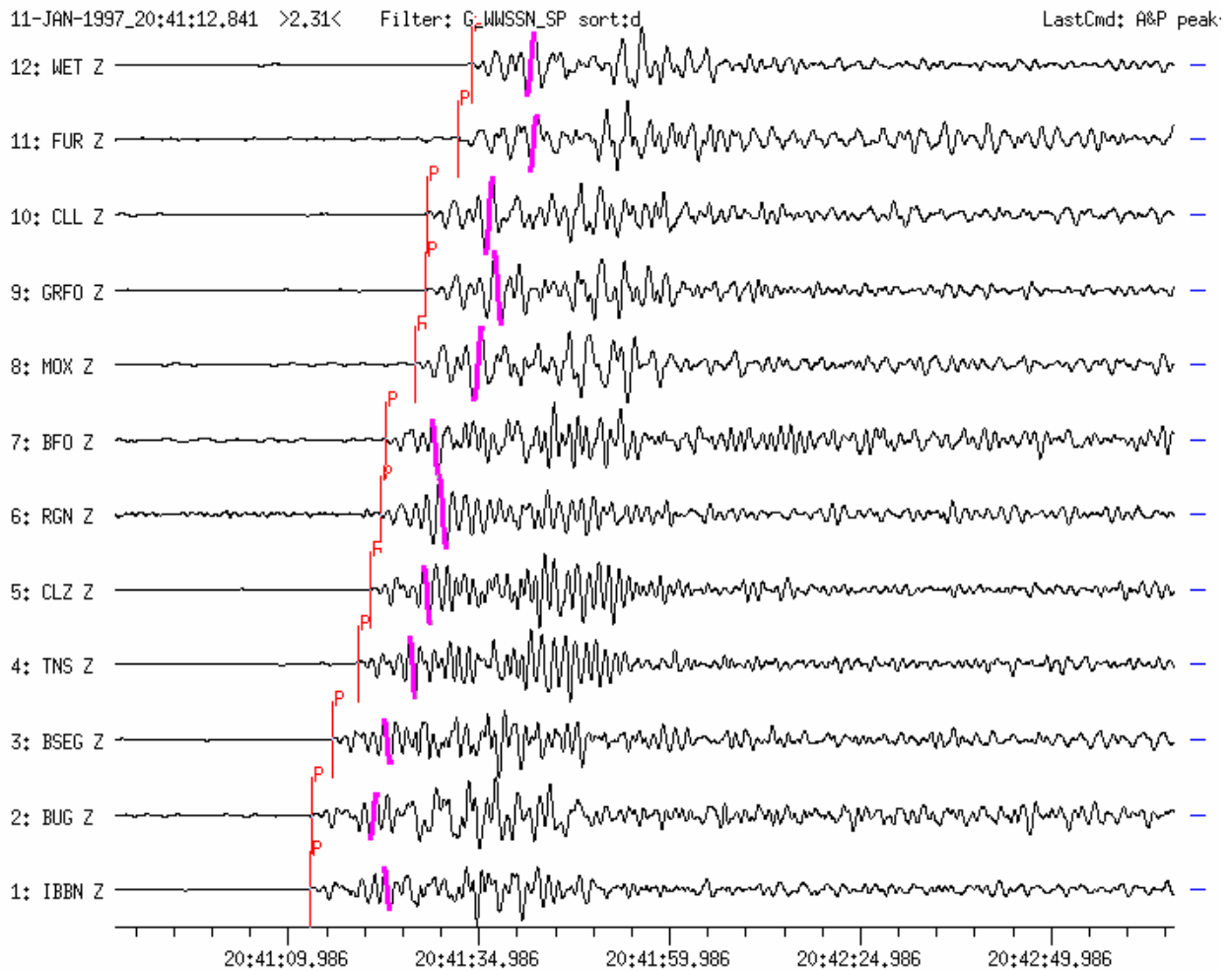


Figure 12b Records at the same stations as in Figure 12a, however after application of a short-period WWSSN-LP simulation filter. This is necessary for amplitude and period measurements required for standardized mb body-wave magnitude determinations. Maximum double-amplitudes ($2A$) and half-periods ($T/2$) are marked for the first wave group. Later onsets may belong to secondary or depth phases.

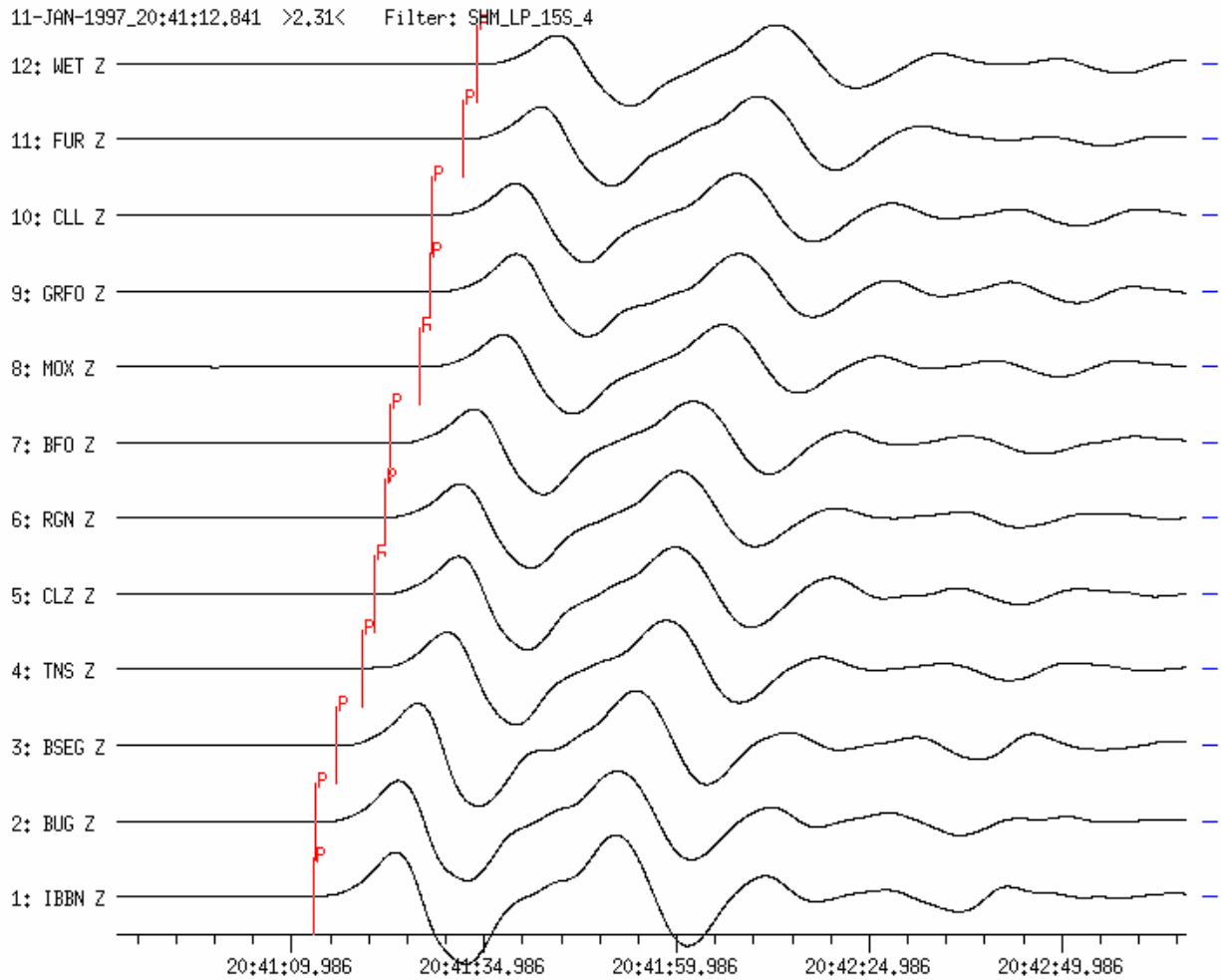


Figure 12c Records at the same stations as in Figure 12a, however after application of a 4th-order Butterworth low-pass filter ($f_c = 15$ s). They show the long-period energy content of the earthquake with P-wave periods of about 20s! All long-period network traces are coherent. In this case the network can be used as an array.

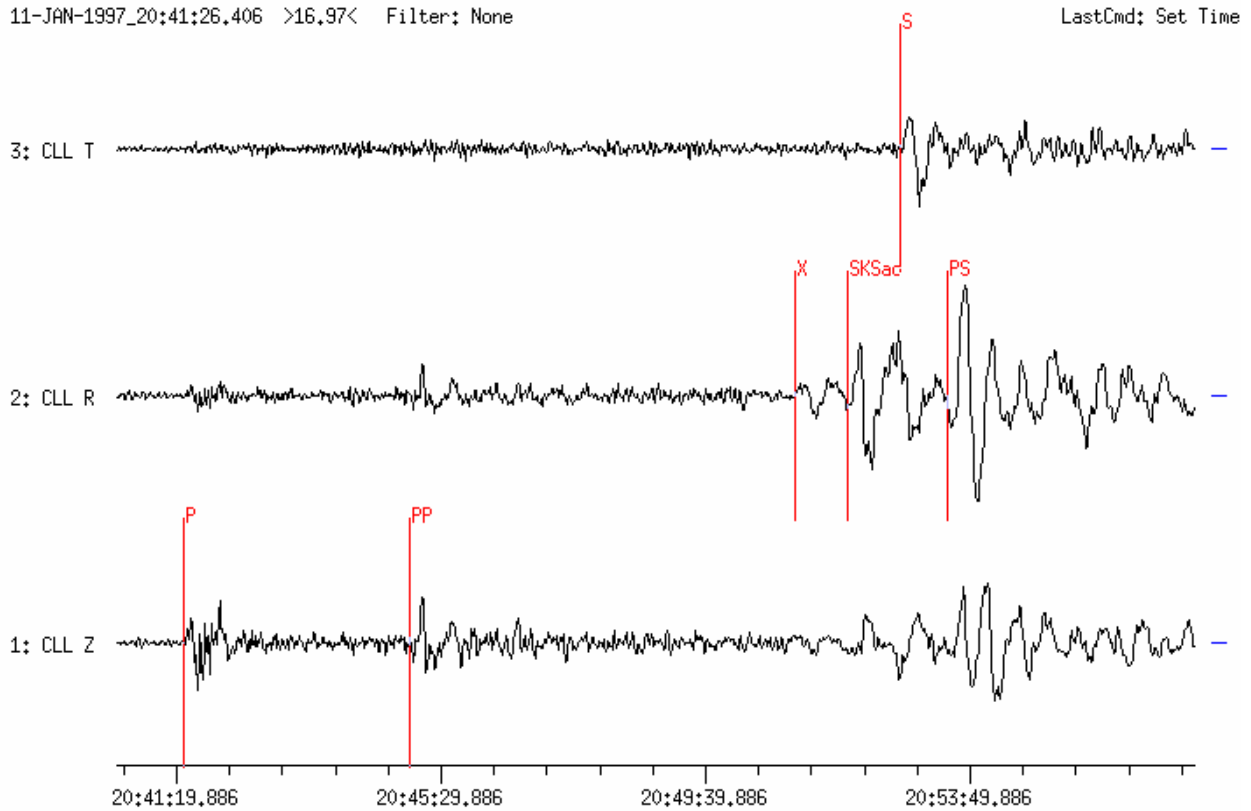


Figure 12d Broadband three-component seismogram recorded at station CLL ($D = 91.0^\circ$, $BAZ = 301^\circ$). Note that at teleseismic distances P waves and their multiples show up most clearly in the Z component because of the small incidence angle, decreasing with distance, and the oscillation of P waves in ray direction. The horizontal components are rotated, with R into the source direction. The radial component shows most clearly the direction of wave propagation (or toward the source; i.e., with a 180° ambiguity which can be resolved by taking the direction of P-wave first-motion – up or down – into account; see EX 11.2). Accordingly, in the R component all waves show up clearly which are polarized in the Z-R plane. These are, besides the primary and multiple P waves also all waves which have been converted during their propagation at discontinuities from P into S and vice versa such as PS, PPS, SP, SSP etc. but also SKP, PKS, SKS, SKKS etc. The latter had to travel at least one segment along their travel path through the Earth’s outer core (K) which is liquid and transmits no S waves. S waves, however, which have been generated by mode conversion from P waves, can oscillate only in the same Z-R plane as P itself. And when a mantle S waves hits the core-mantle boundary, only their vertically polarized SV energy can partially be converted into a P wave and penetrate into the outer core while any SH energy will be totally reflected back into the mantle. This also explains, why multiple S-wave reflections such as SS, SSS, SSSS contain an increasing part of SH energy. The primary S waves, as originating from the earthquake rupture process, may contain both SV and SH energy in variable proportions, depending on the rupture orientation in space. The SH part shows up in records of the transversal (T) component. When comparing energy arrivals in the S-wave time window in the T and R components one can discriminate between S and SKS (see figure above). Note that SKS and PS are recorded also in Z, however with smaller amplitudes because of their oscillating perpendicular to the ray orientation. An unknown phase, denoted X, appears ahead of SKS in R. Surface waves are not visible because they arrive outside of the displayed time window.

For single station analysis phases can be determined with the help of (differential) travel-time curves (see Figure 2 in Exercise EX 11.2). For a station network vespagram analysis (see also Chapter 9, section 9.7.7) proves to be a much better analysis method because of the additional slowness determination. The following three figures (12e - 12g) show vespagrams of the vertical (Z), radial (R) and transverse (T) components recorded at 12 GRSN-stations. To get a better signal coherency, all traces were filtered with a 4th- order long-period low-pass filter ($f_c = 15$ s).

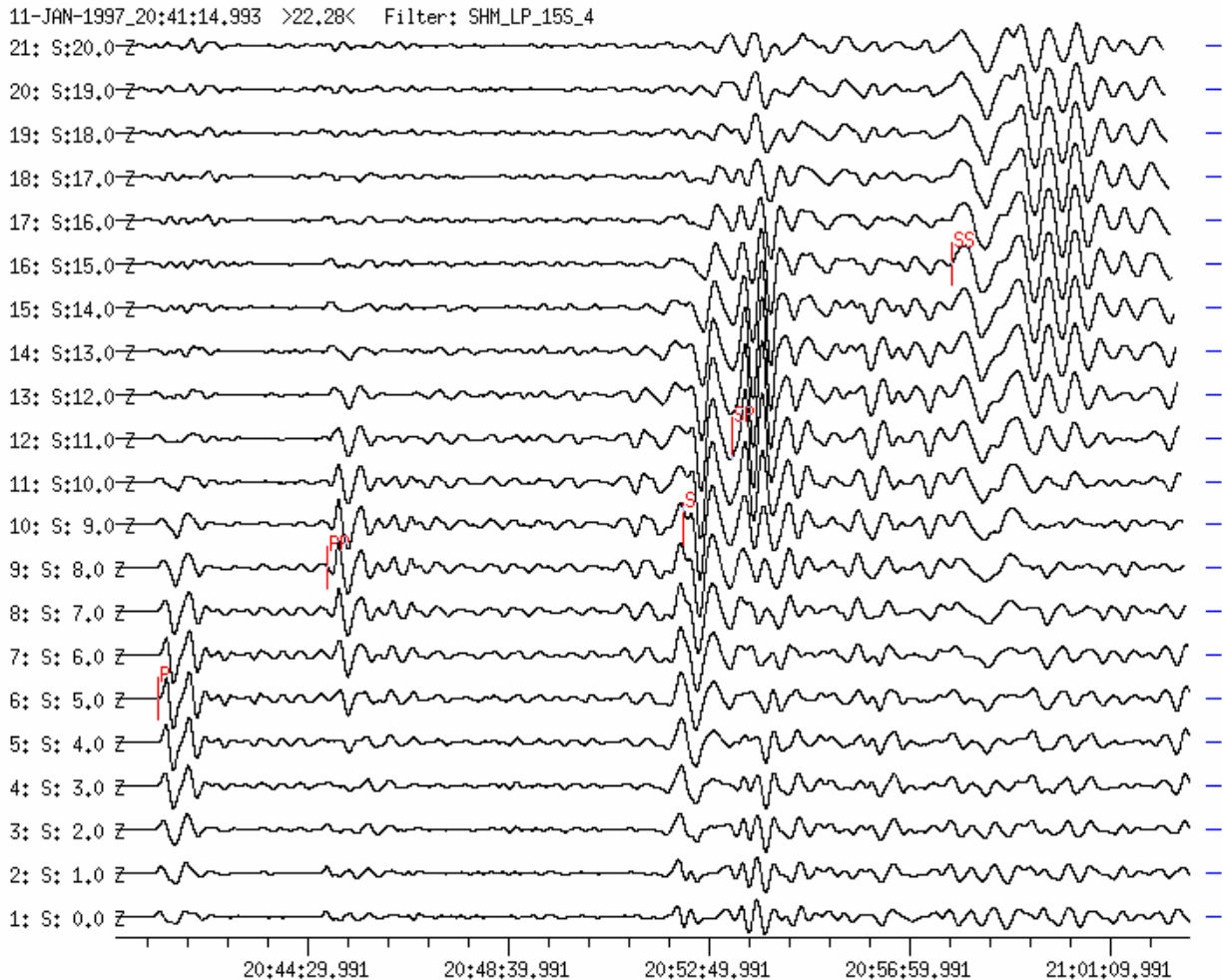


Figure 12e The identified phases from the vertical-component vespagram are marked on the respective slowness traces where they have their largest amplitudes (e.g. P on trace 6: belonging to a slowness $S = 5$ s/ $^\circ$, PP on trace 9 with $S = 8$ s/ $^\circ$, SP on trace 12 with $S = 11$ s/ $^\circ$ and SS on trace 16 with $S = 15$ s/ $^\circ$).

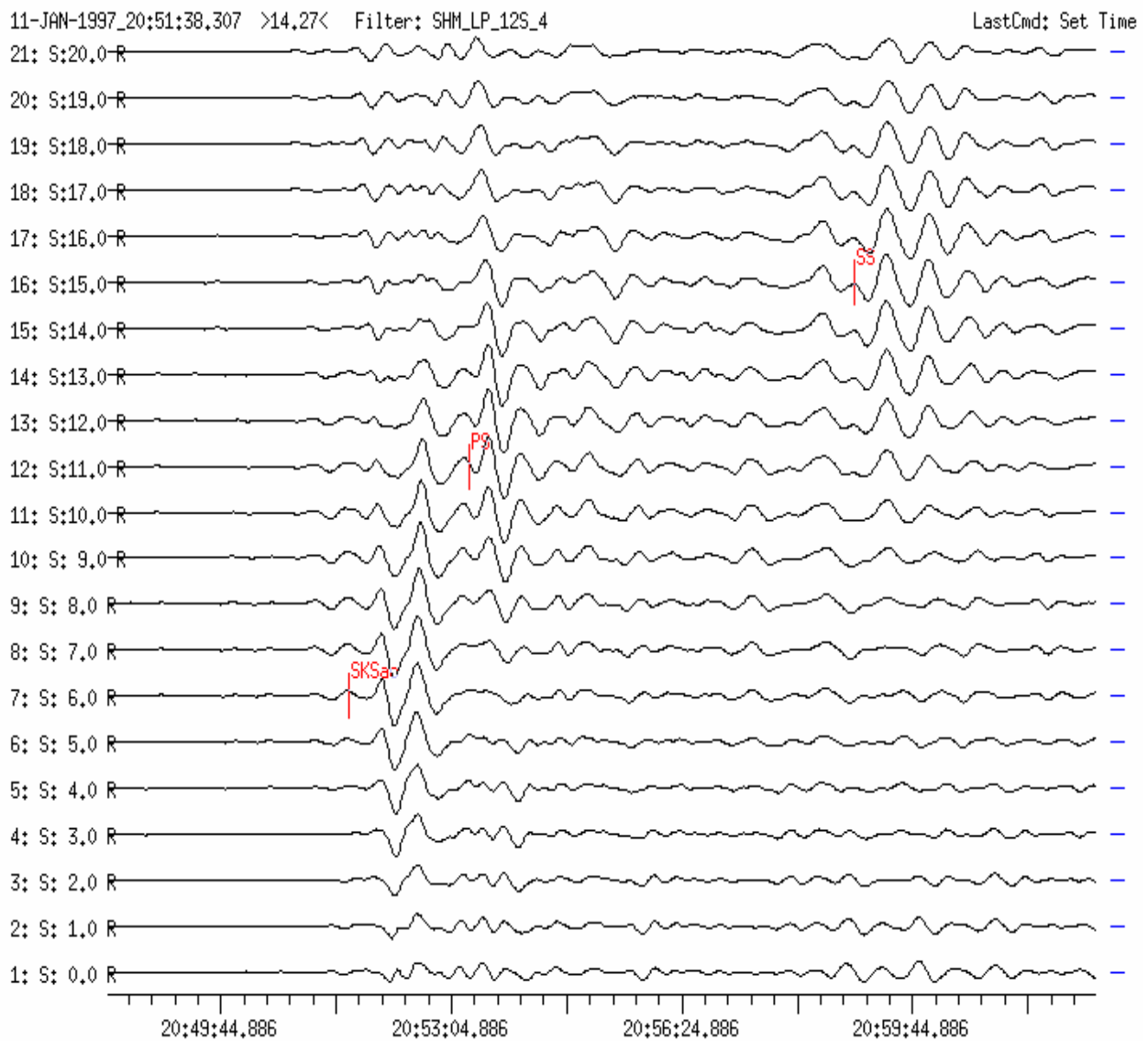


Figure 12f The identified phases from the radial-component vespagram are marked on slowness the respective slowness traces (SKSs on trace 7 with a slowness $S = 6 \text{ s}^\circ$, PS on trace 12 with $S = 11 \text{ s}^\circ$ and SS on trace 16 with $S = 15 \text{ s}^\circ$).

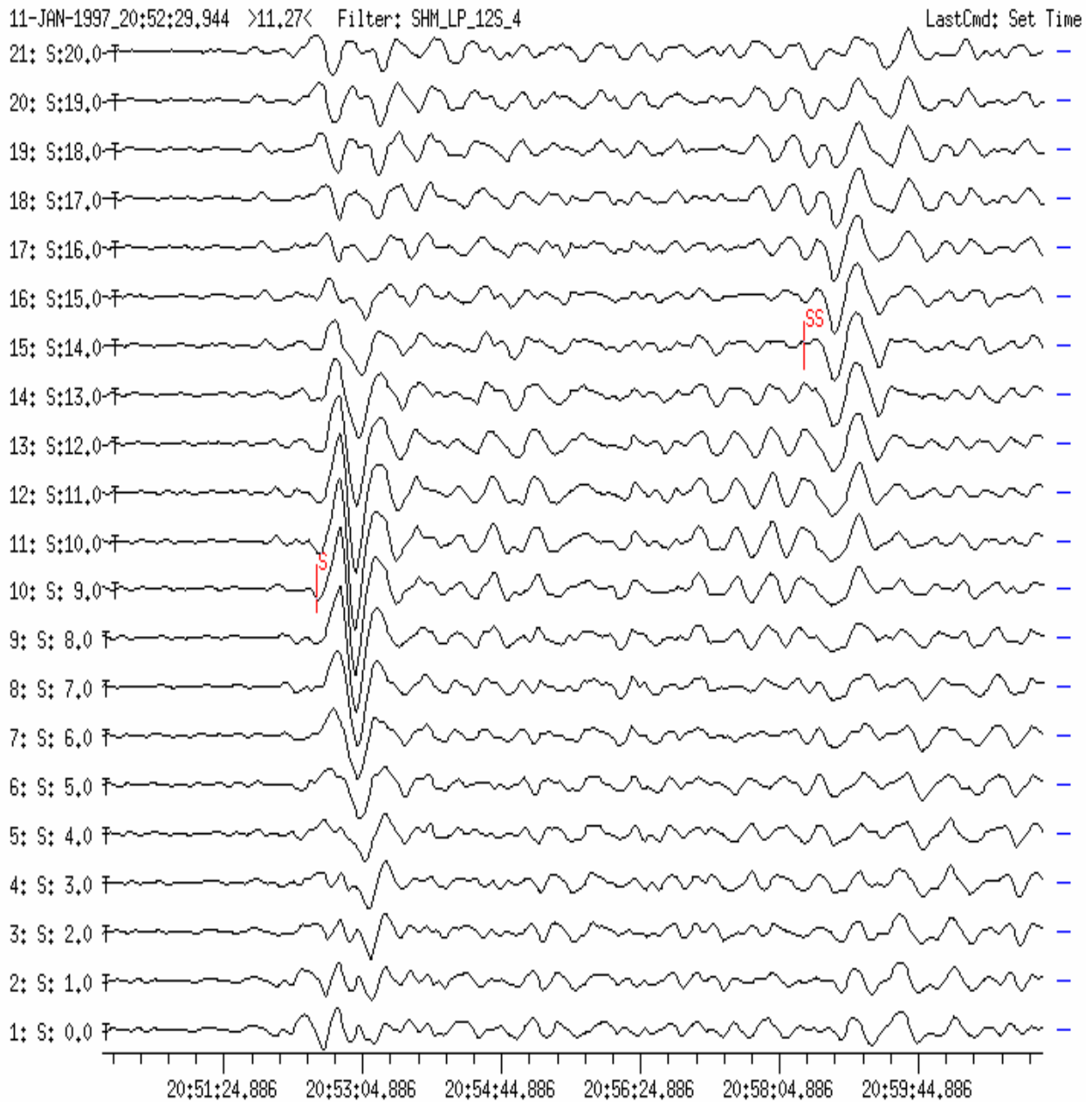


Figure 12g The identified phases from the transverse-component vespagram are marked on their respective slowness traces (S on trace 10 corresponding to a slowness $S = 9 \text{ s}^\circ$, SS on trace 15 with $S = 14 \text{ s}^\circ$). Note, by comparing the identifications in Figs. 12e to 12g that the associated slowness values might somewhat differ because the maximum amplitudes vary only slightly when changing the slowness for about ± 1 or 2 s° .

Example 13: Earthquake near the coast of Ecuador

USGS NEIC-data: 1998-08-04 OT 18:59:18.2 0.551S 80.411W h = 19G
 mb = 6.2 Ms = 7.1 (D = 91.5° and BAZ = 270.9° from GRF(GRA1))

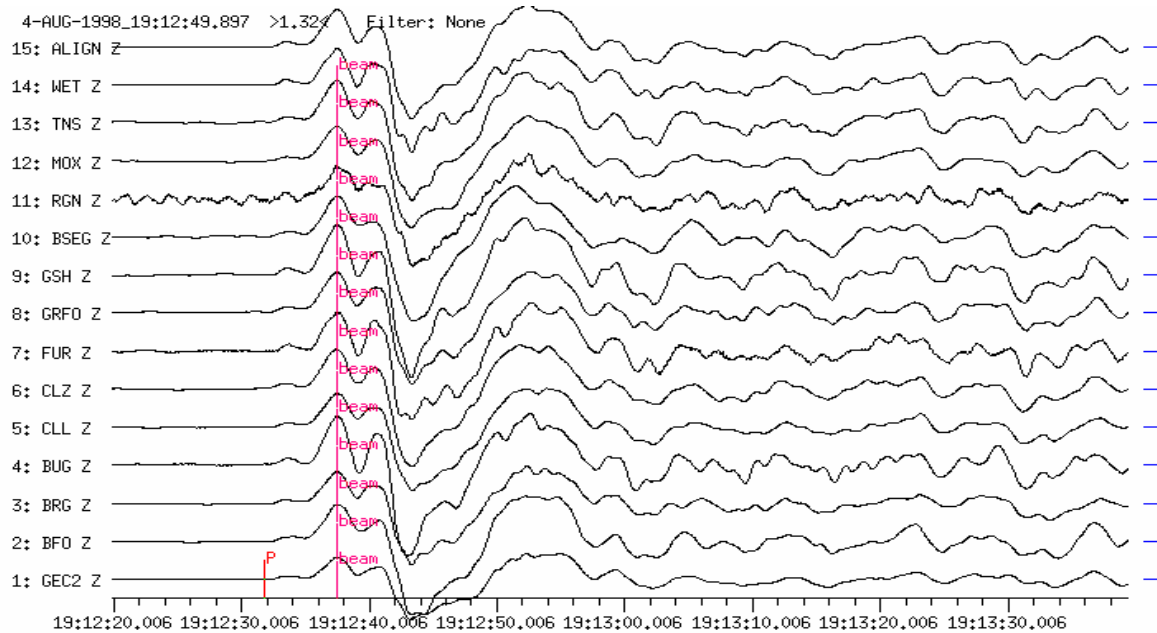


Figure 13a Broadband vertical-component seismograms recorded at 14 GRSN stations (D = 88.4° to 93.2°). Traces are time-shifted and aligned. The different waveforms observed at different network stations are coherent in the long-period range.

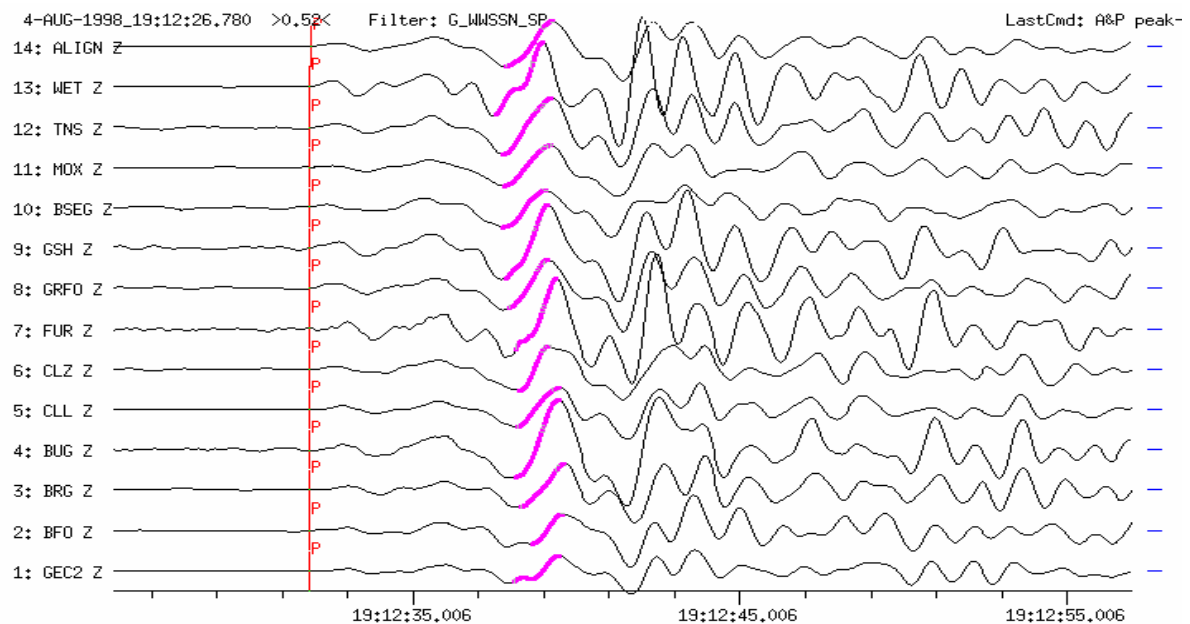


Figure 13b: After short-period filtering (WWSSN-SP simulation) the coherency of the different station-waveforms is bad. The maximum double P-amplitudes used for mb-estimation are emphasized. Because of the variability of station amplitudes within the network individual mb-values vary between 6.0 for BFO and GEC2 and 6.7 for other stations.

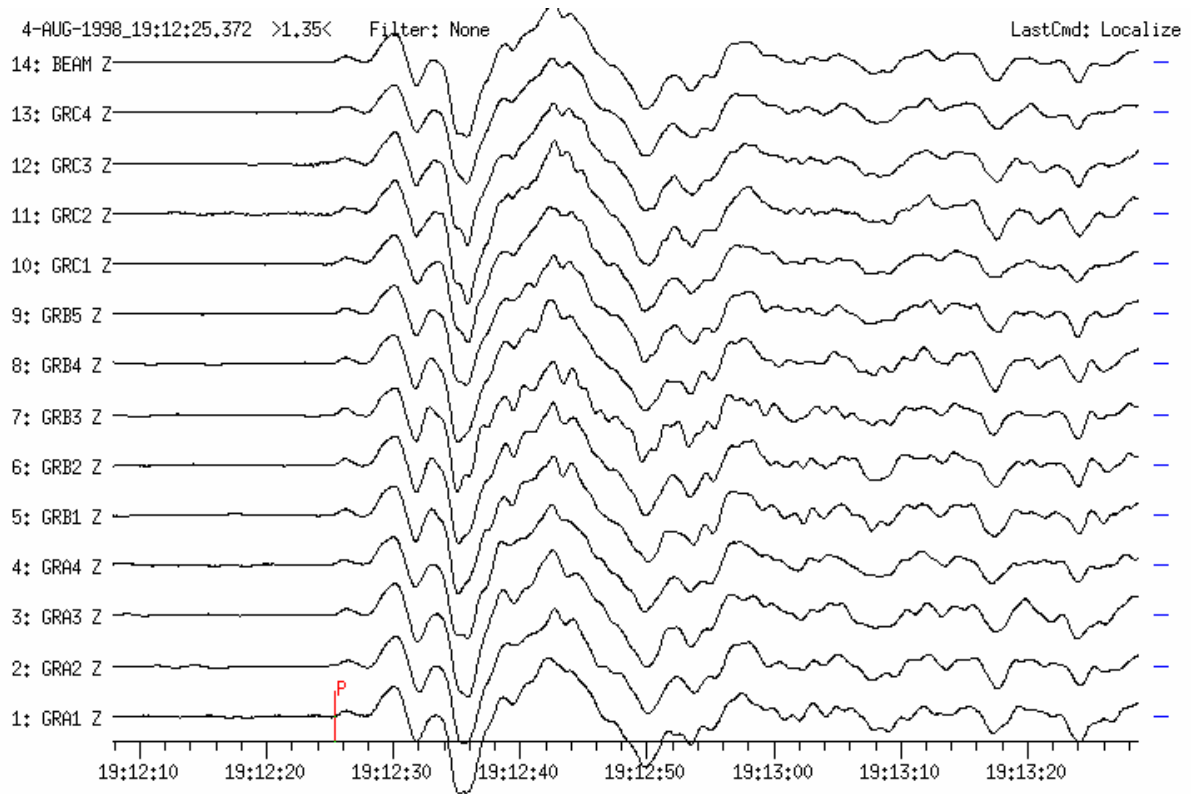


Figure 13c Broadband records of the vertical-components at 13 GRF-array stations ($D = 91.5^\circ$ to 91.7°). Because of the much smaller aperture of the array as compared to the GRSN the signal coherence is good for all array-traces.

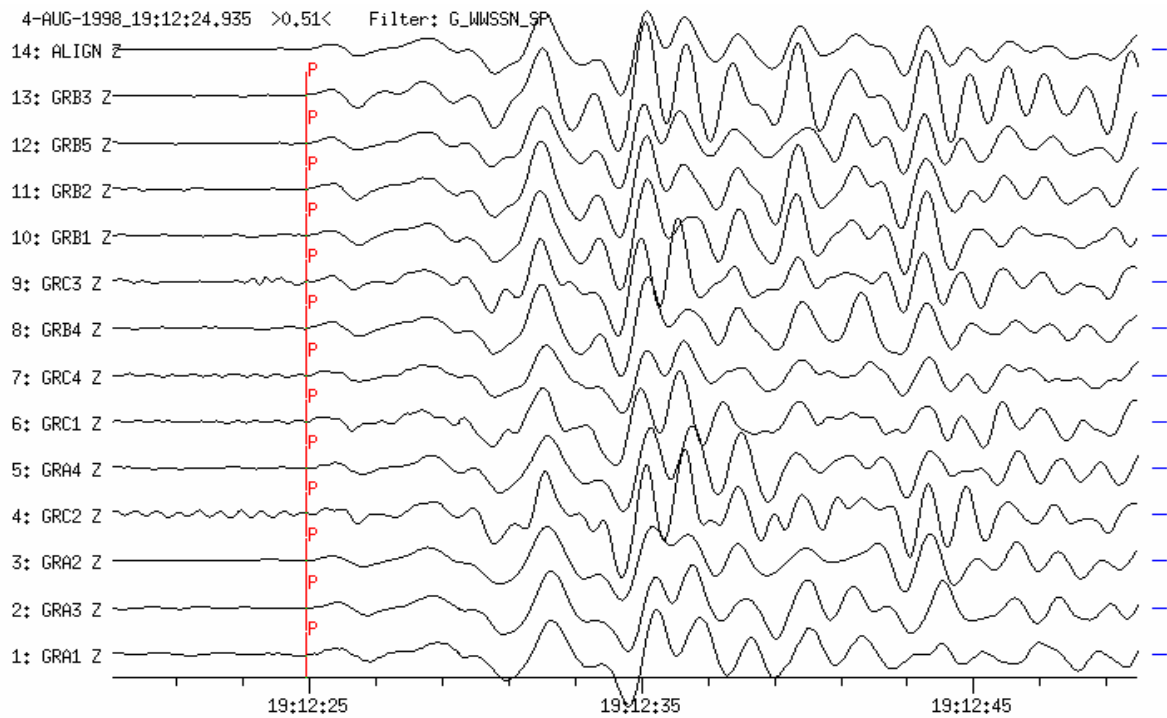


Figure 13d Even for the short-period filtered records of the GRF-array stations (WWSSN-SP simulation) the signal coherence is still good.

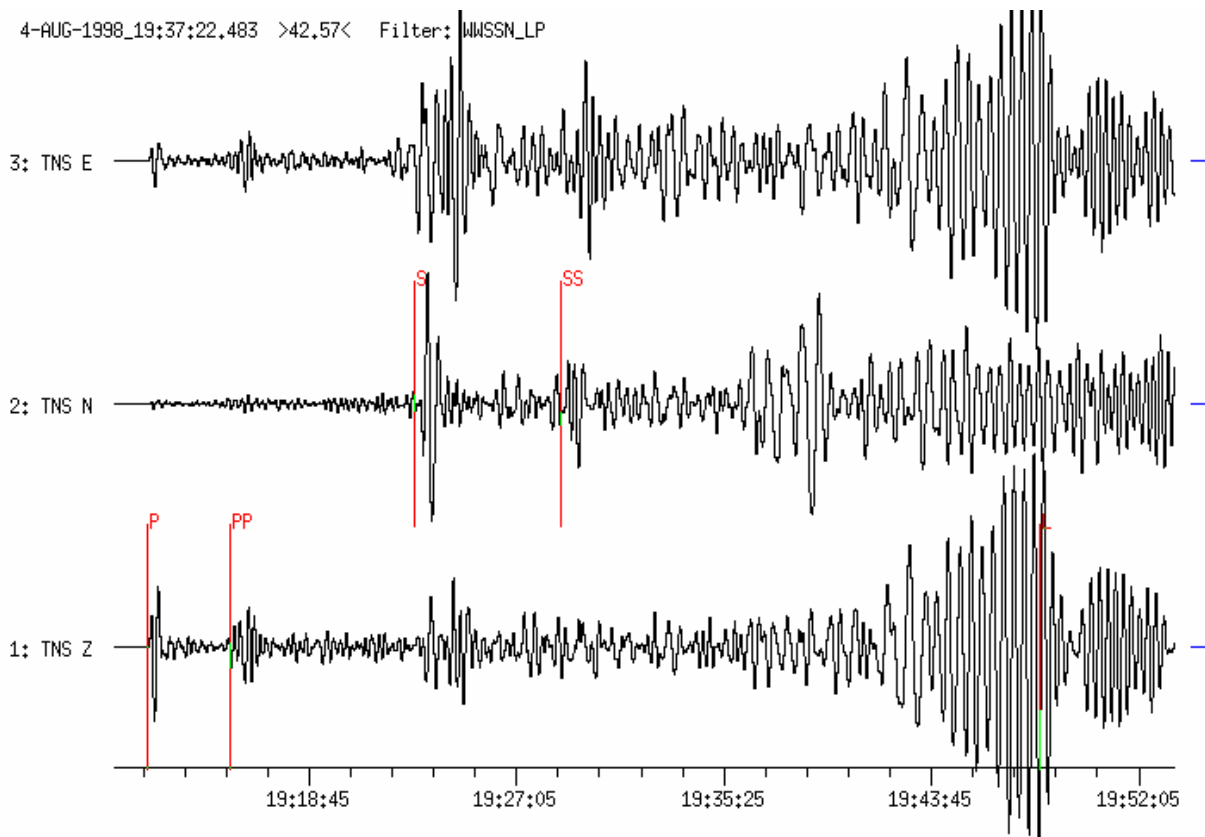


Figure 13e Three-component long-period filtered (WWSSN-LP simulation) seismogram recorded at station TNS ($D = 89.7^\circ$, $BAZ = 269^\circ$). Note the much larger P-wave amplitude in the E-W component as compared to the N-S component because of the source location in the west. Also note the strong secondary phases PP, S and SS. The maximum surface-wave amplitude on the vertical component is marked (L). The estimated magnitude is $M_s = 7.2$. This is very close to the average value determined by the USGS NEIC from data of the global seismic network ($M_s = 7.1$).

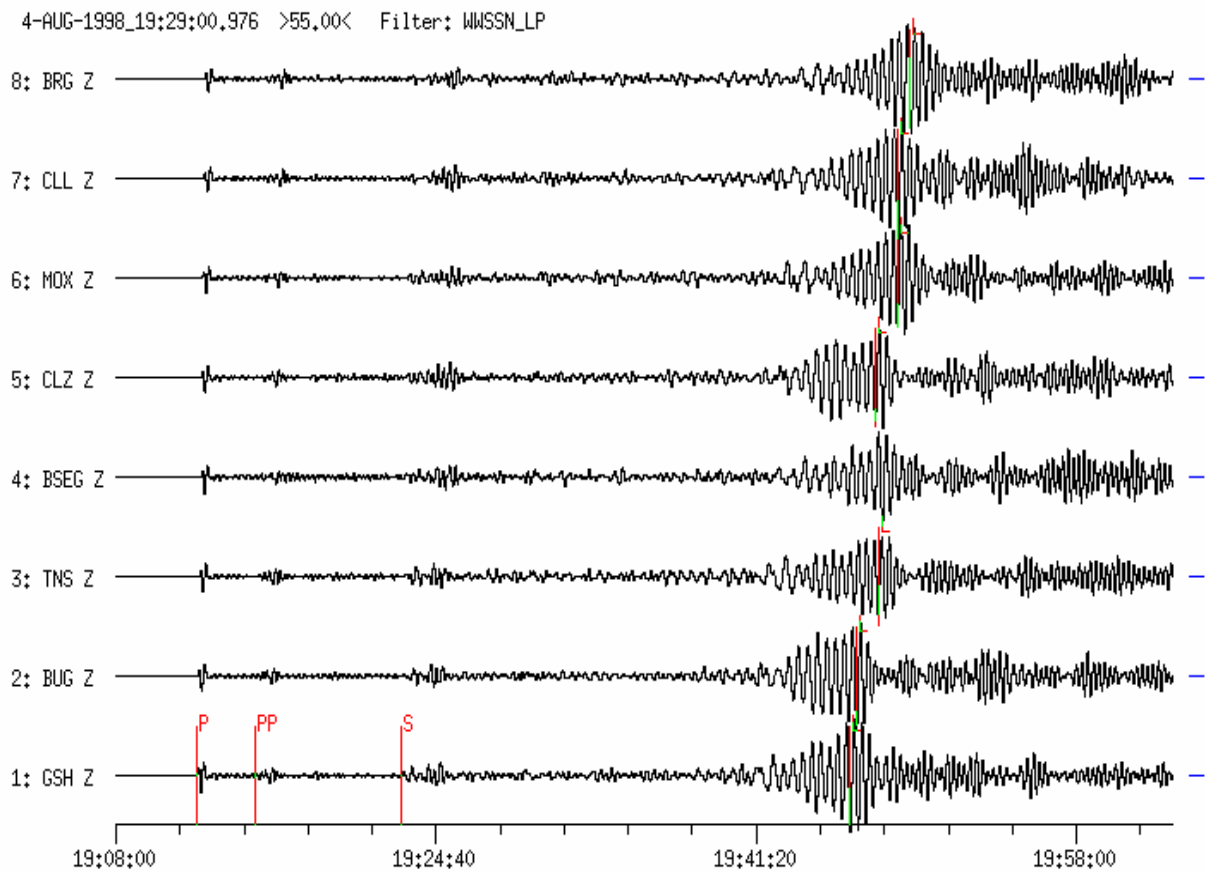


Figure 13f Long-period filtered (WWSSN-LP simulation) vertical-component records of the Ecuador earthquake at 8 GRSN stations within the distance range $D = 88.4^\circ$ (GSH) to 93.2° (BRG). The variability of the maximum surface-wave amplitudes throughout the network is less than that of short-period body-wave amplitudes (compare with Figure 13b). Accordingly, M_s estimates from individual stations are more reliable than respective m_b estimates.

Example 14: Earthquake in Southern Sumatra Region

USGS NEIC-data: 2000-06-04 OT 16:28:25.8 4.773 S 102.050 E h = 33G
 mb = 6.8 Ms = 8.0 (D = 94.1° and BAZ = 92.5° from GRF)

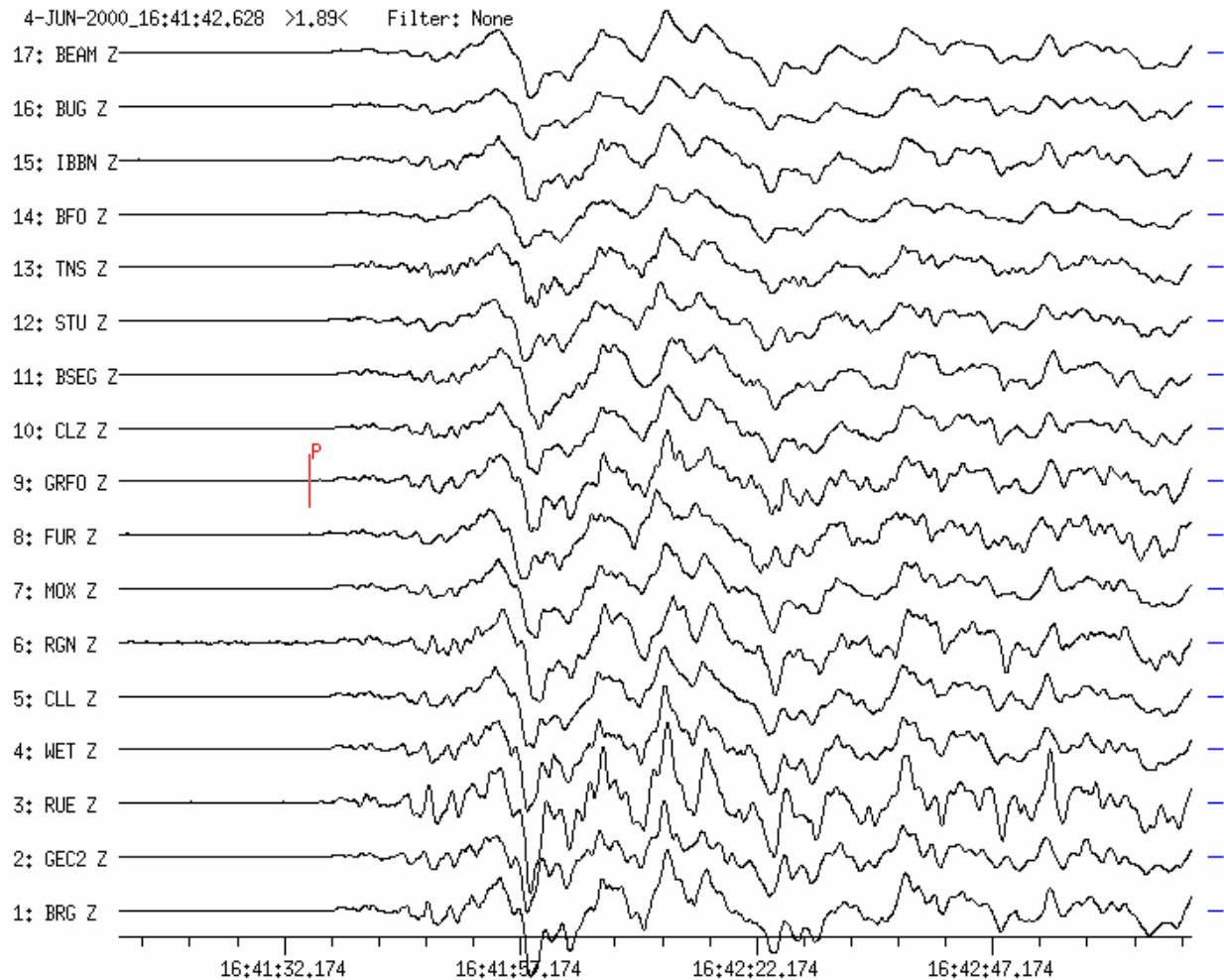


Figure 14a Broadband vertical-component seismograms recorded at 16 GRSN-stations within the distance range $D = 92.5^\circ$ to 96.7° . Traces are time-shifted and aligned for better comparison of the individual records. Note the good coherency of all traces. For these broadband records the network works like an array. The weak P-wave first arrival is marked on the record of station GRFO. Maximum P-wave amplitudes were recorded about half a minute later (multiple rupture event with successively larger energy release?).

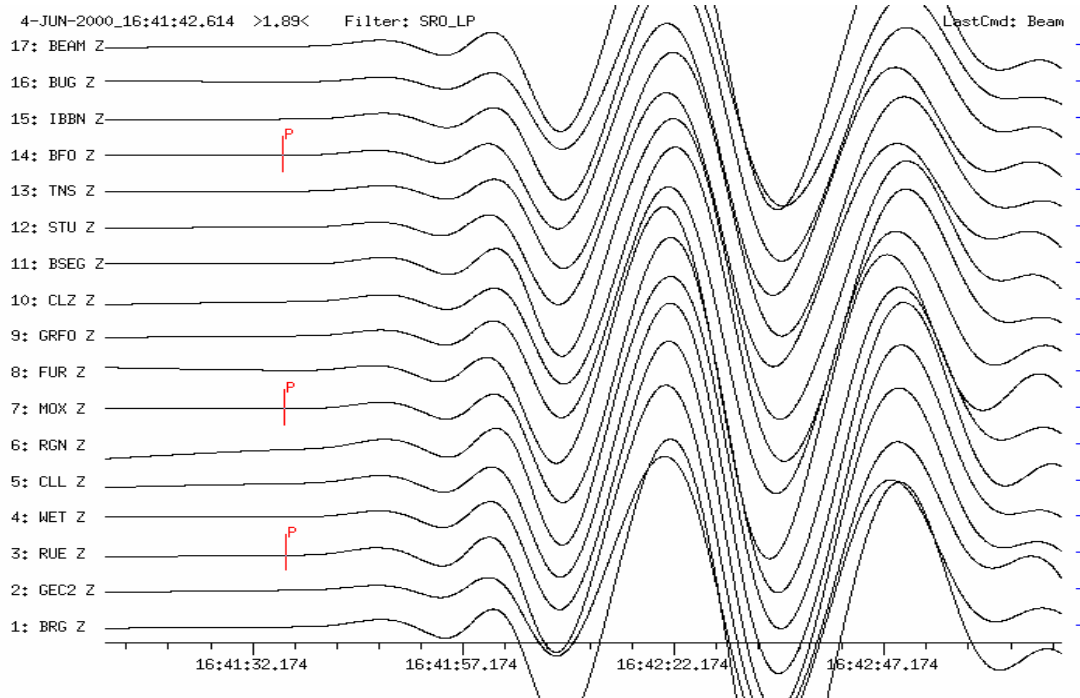


Figure 14b Seismograms of the same earthquake recorded at the same stations as in Figure 14a after applying a long-period filter (SRO-LP simulation). Note the very high signal coherence of the long-period P-waves with periods $T \approx 25$ s. Also the amplitudes are comparable at all stations.

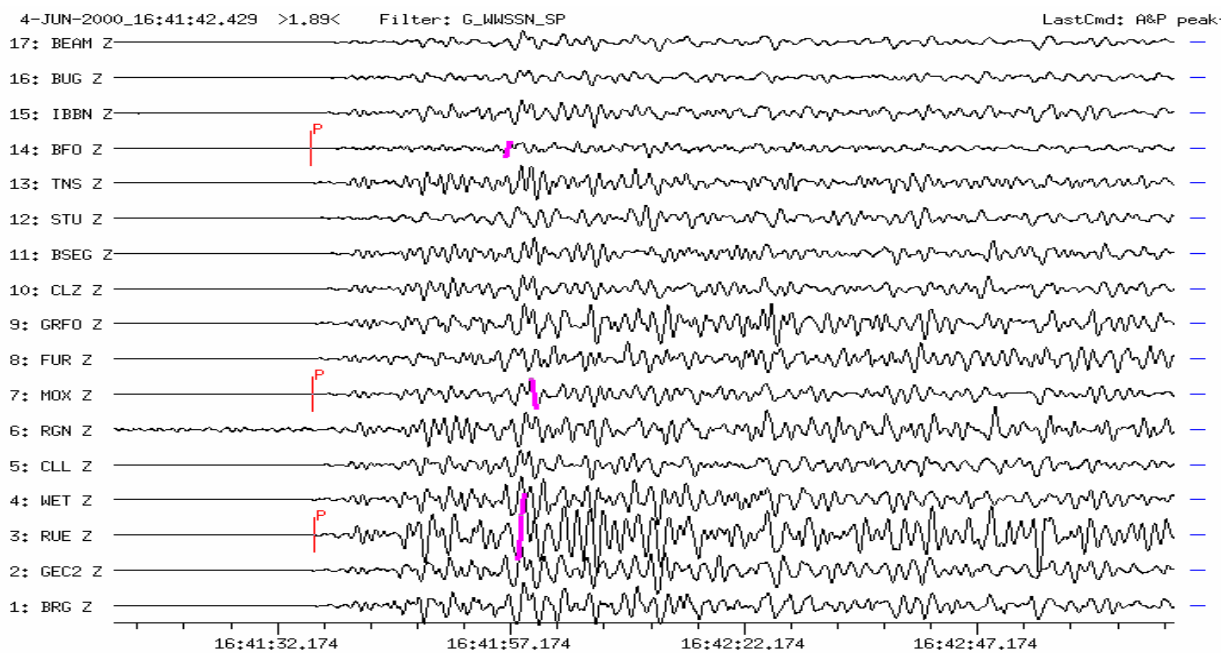


Figure 14c For mb estimates short-period records (WWSSN-SP simulation) have to be used to measure the maximum amplitudes with periods near 1 s. The respective filtered traces for the same earthquake and stations as in Figure 14a are shown. For three stations the P wave arrivals and their maximum double-amplitudes $2A$ have been marked. The latter differ by a factor of five for this event. This corresponds to a difference of 0.7 magnitude units!

4-JUN-2000_16:41:41.368 >1.10< Filter: G_WWSSN_SP

LastCmd: A&P peak

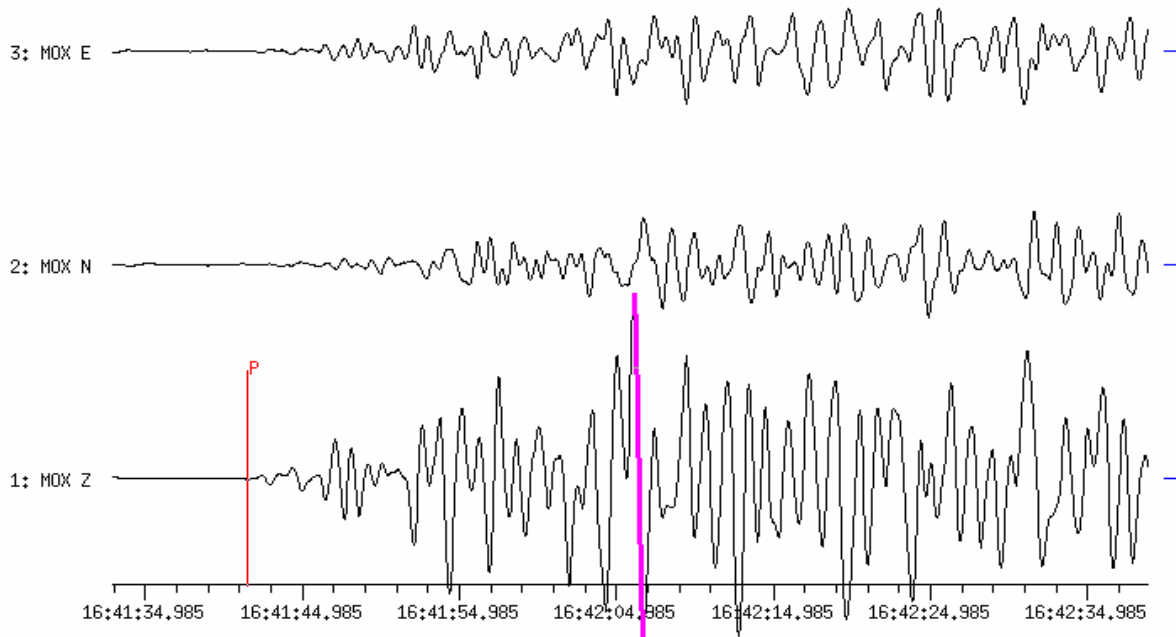


Figure 14d Three-component single station record of the Sumatra earthquake at station MOX ($D = 93.9^\circ$, $BAZ = 93^\circ$). The short-period filtered P-wave group is shown and the maximum peak-to-peak amplitude $2A$ is marked as in the Z component. In this display with high time resolution the complicated rupture process of this event, consisting of a series of sub-events with successively increasing energy release within the first 25 s is very obvious. This is a very important information also for more detailed research work on source processes. Therefore, also for routine data analysis a detailed reporting of the onset times, amplitudes and periods of these sub-events is strongly recommended. An example for such an analysis is given in Tab. 3.1 of Chapter 3. In the given case, the amplitude of the P-wave maximum around 16:42:06 is about 40 times larger than that of the first arrival. This corresponds to a difference of 1.6 magnitude units between the initial and the largest sub-event of this earthquake. Accordingly, instructions for mb measurements within the first five half-cycles (NOAA in the 1960s) or within the first 5 s (IMS nowadays) might dramatically underestimate not only the energy release of earthquake in general (stronger ones in particular, because mb will always saturate at values around 6.5; see Figs. 3.5 and 3.16 and related discussions in sections 3.1.2.3, 3.2.5.2, and 3.2.7 of Chapter 3). Even worse, they will particularly underestimate the high-frequency energy release which is most relevant for potential damage assessments and for these mb is principally more suited than M_s or M_w provided, that mb is determined really from the maximum amplitudes in short-period P-wave train.

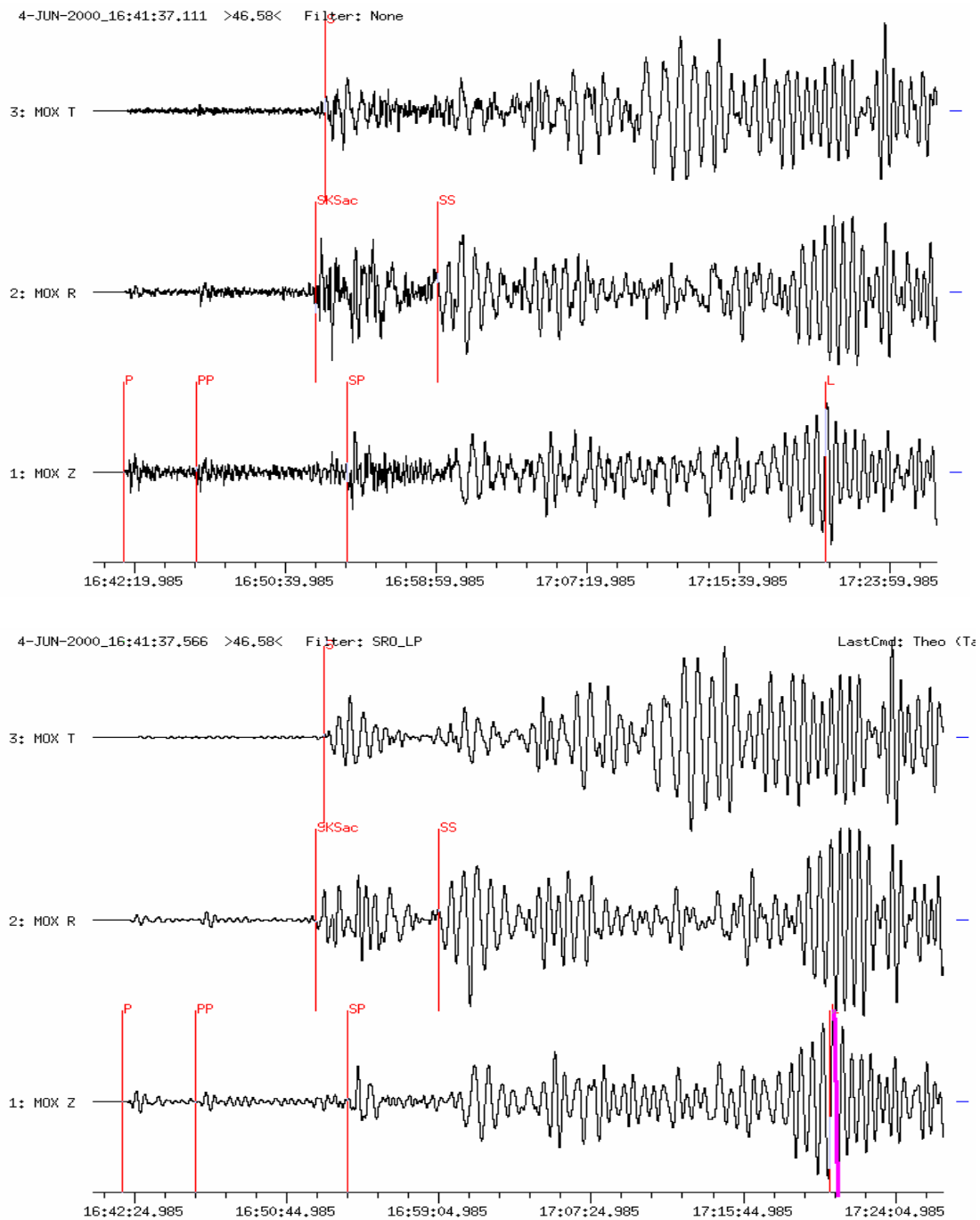


Figure 14e Broadband (top) and long-period filtered 3-component seismograms (SRO-LP simulation; below) of the Sumatra earthquake at station MOX ($D = 93.9^\circ$). The phases P, PP, S, SKSac, SP, SS and the maximum surface wave L have been marked. For better phase identification the horizontal components N and E have been rotated into the R and T directions. The S wave is seen best on the transversal component T and P, PP, SKS and SP on Z and on the radial horizontal component R, respectively. For surface-wave magnitude estimation the maximum ground displacement with a period between 18 and 22 s was measured at the marked position L from the SRO-LP filtered vertical component. Additionally, amplitudes from the horizontal components can be used for a horizontal surface-wave magnitude value.

Example 15: VOLCANO ISLANDS REGION

USGS NEIC-Daten: 2000-03-28 OT 11:00:21.7 22.362N 143.680E h = 119D
 mb = 6.8 (D = 96.8° BAZ = 43.5° from GRF(GRA1))

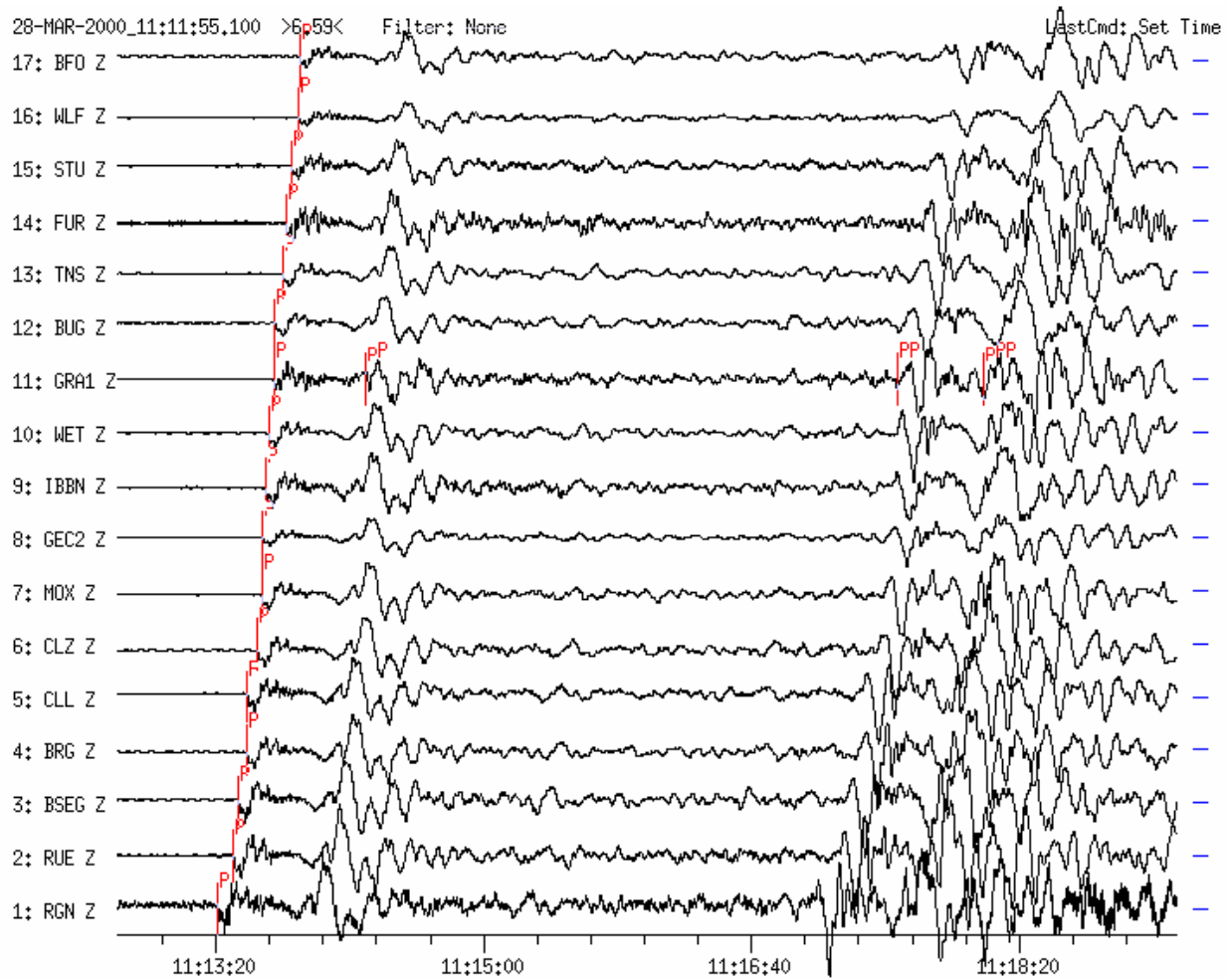


Figure 15a Broadband vertical-component seismograms recorded at 17 GRSN-, GRF- and GEOFON-stations. Traces are sorted according to increasing distance (D = 92.4° to RGN and 99.1° BFO). The phases P, PP and the depth phases pP and pPP are recorded very well.

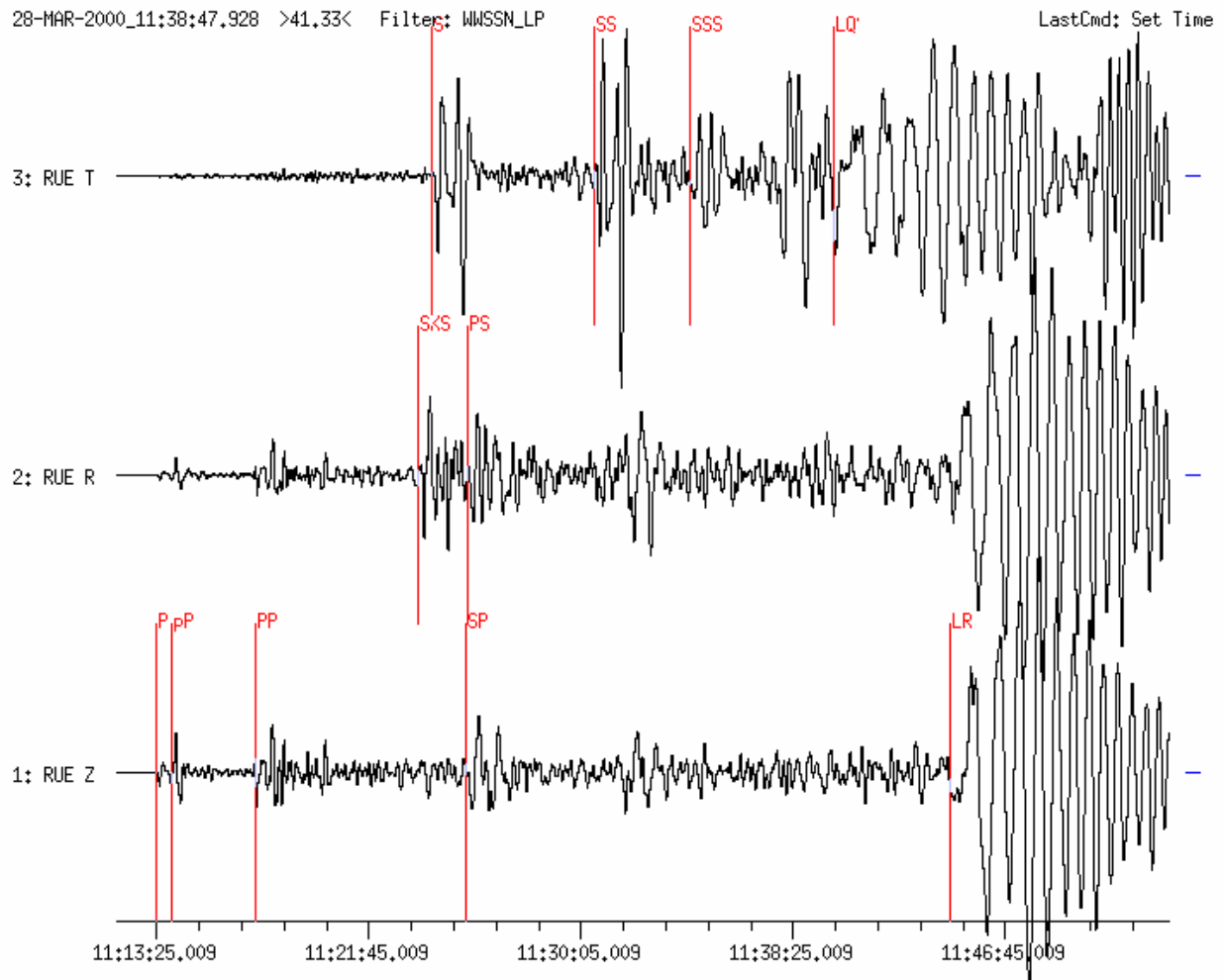


Figure 15b Long-period filtered (WWSSN-LP simulation) three-component seismogram of the Volcano Island earthquake recorded at station RUE near Berlin ($D = 93.7^\circ$, $BAZ = 45^\circ$). The horizontal components are rotated, with R in source direction. Phases P, pP, SP and the onset of the Rayleigh waves LR are marked on the vertical component, SKS and PS on the radial component and S, SS, SSS as well as the Love waves onset LQ on the transversal component, respectively.

